The Two-layer Skirted Island

by

Joseph Pedlosky[1,2]

Roberto Iacono[3]

Ernesto Napolitano[3]

and

Michael A. Spall[1]

February 28, 2011

1. Woods Hole Oceanographic Institution

Woods Hole, MA 02543, USA

2. Corresponding author: ***email: jpedlosky@whoi.edu***

3. ENEA, C.R. Casaccia, Rome, Italy

Abstract

The flow around a planetary scale island in a baroclinic ocean is examined when the island possesses a topographic skirt representing a steep continental slope and the ocean is modeled as a two-layer system in order to examine the role of stratification in the circulation. The study extends an earlier barotropic model of similar geometry and forcing to focus on the degree to which the topography, limited here to the lower of the two layers, affects the circulation and to what degree the circulation is shielded by stratification from the topographic effects noted in the simpler barotropic model.

As in the barotropic model, the topography is steep enough to produce closed, ambient potential vorticity contours over the topography in the lower layer providing free "highways" for the deep flow in the presence of small forcing by the wind-driven upper layer flow. The flow is very weak outside the region of closed contours but can become of the same order, if somewhat smaller, as the upper layer flow on those contours in the presence of even weak coupling to the upper layer.

A series of models, analytical and numerical, are studied. Linear theory is applied to two configurations. The first consists of a long, meridionally oriented island with a topographic skirt in the lower layer. The lower layer flow is driven by a hypothesized frictional coupling between the two layers that depends on the circulation of the upper layer velocity on a circuit defined by the closed potential vorticity contours of the lower layer. The largest part of the driving flow is identical on both sides of the island and cancels in the contour integration. The major part of the residual forcing comes from relatively small but effective forcing on the semi-circular tips of the topographic skirt. A circular island with a topographic skirt is also examined in which the coupling to the

upper layer is stronger all around the island. Even in this case there is a delicate balance of the forcing of the lower layer on each side of the island. In all cases the flow on closed potential vorticity contours in the lower layer is much weaker than in the barotropic model but much stronger than in the flat region of the lower layer.

A sequence of numerical calculations that both check and extend the analytic linear theory is presented demonstrating the subtlety of the force balances. Further nonlinear, eddy-containing experiments give a preview of the direction of future work.

1. Introduction

In a recent paper, Pedlosky *et al.* (2009), hereafter PINH, considered the flow around a planetary scale island when the island possesses a topographic skirt that girdles the island and crudely represents a continental slope. Of particular interest was the change in both the structure of the circulation near the island and the way in which Godfrey's (1989) "Island Rule" must be reinterpreted. The presence of isolines of ambient potential vorticity, f/h, where f is the Coriolis parameter and h is the depth of the single, constant density layer of the model, completely alters the form of the circulation. It eliminates the recirculation found in theories of flat bottom oceans (Pedlosky *et al.* 1997) and traps a relatively strong circulation around the potential vorticity (pv) contours that does not participate in the basin-wide circulation and suggests that the Island Rule should instead be applied to the domain demarked by the outermost closed pv contour instead of the boundary of the island's surface expression. The strong circulation on the closed pv contours represents a steady resonance, that would exist in a frictionless fluid, of the free geostrophic mode on those contours. The resonance, forced by the wind stress in the model, is bounded ultimately by the weak dissipation in the system and so is able to reach large velocities.

It is naturally of interest to reconsider the problem to take into account the baroclinic character of the ocean circulation and to examine to what extent the ideas of the barotropic model of PINH remain valid when the topography is shielded from the direct forcing by the wind by an overlying layer of lower density. We take up this

problem in a two-layer model to keep our model, both analytic and numerical, as simple as possible. In this paper the topography will be limited to the region of the lower, second layer although we shall discuss qualitatively some results for larger topography that penetrates into the upper layer. Although there have been studies examining the island effect in baroclinic ocean models (e.g. Pedlosky 2010, Spall 2000) the joint effect of topography and stratification renders the dynamics considerably more complex.

Section 2 describes the basic model and the model equations which are essentially a two-layer version of the dynamics in PINH. Section 3 describes the basic model geometries and the results of linear theory for the two geometries considered, i.e. the meridional, thin island and skirt and the circular island with its skirt that girdles the island. In both cases the topography introduces closed isolines of potential vorticity in the lower of the two layers. The forcing of the lower layer flow is shown to be much less efficient for the meridionally oriented island over most of its length. Nevertheless, effective forcing over a relatively small domain near the two meridional extremes of the topography dominate the forcing and are sufficient to drive a substantial flow along the pv contours in the lower layer. The circular island is studied as an example of a geometry where the forcing is more effective over a larger portion of the skirt. Section 4 presents our numerical results and compares them with the results of our simple analytical theory and this serves to underline the delicate nature of those analytical results reflecting the subtle balances that obtain in the dynamics. Section 5 presents some preliminary results where layer coupling is due to spontaneously generated eddies. In section 6 we summarize and discuss our results.

2. The model

Figure 1 shows a definition sketch of the first model we are using. The first panel shows a zonal cross section of the island and its topography. In the upper layer it is a very thin island oriented in the north-south direction for $y_s \le y \le y_n$. The height of the peak of the topography from the otherwise flat bottom is h_T, and it extends a distance x_T to each side of the island. The local thickness of the second layer is h_2 while the layer thicknesses beyond the topography are, in the absence of motion, H_1 and H_2, both constant. In plan view its topography is shown in Figure 1b while the third panel shows the isolines of ambient potential vorticity, i.e. in the absence of motion, for a skirt width of 250 km, a height above the bottom of 500 m in a layer of thickness 1000 meters which is also the thickness of the upper layer. This relatively short island is 800 km in length. For these parameters there is significant departure of the pv isolines from the topography but we will generally consider cases in which the departure is locally rather small. Even in this case the pv gradient due to the beta effect is ten times smaller that the pv gradient due to the change in layer thickness induced by the topography. Note that the topography has been smoothed within semi-circular regions at the northern and southern tips of the island to avoid abrupt changes in depth.

The second geometry we will examine, shown in Figure 2, consists of a circular island in the upper layer with radius r_I extending into the lower layer in which an azimuthally symmetric, circular skirt extends to radius r_T. The skirted island in both cases is placed at the center of a basin of radius r_o.

The circulation is driven by a wind stress,

$$\vec{\tau} = \rho\tau_o r / r_o \hat{i}_\theta \qquad (2.1)$$

where $\hat{i}_\theta$ is a unit vector in the azimuthal direction. The stress provides a spatially constant curl, $2\tau_o / r_o$. Here r is the radial distance from the center of our circular ocean basin of radius r_o. The mean density, ρ, is included in the definition of the stress to simplify the formulae that follow so that τ_o has the dimensions of a velocity squared. For our governing equations we take, for each layer,

$$\frac{\partial \vec{u}_n}{\partial t} + (\zeta_n + f)\vec{k} \times \vec{u}_n = -\nabla B_n + \frac{\vec{\tau}}{h_1}\delta_{n1} + \vec{D}_n(\vec{u}_1, \vec{u}_2), \quad n = 1,2$$

$$\frac{\partial h_n}{\partial t} + \nabla \bullet (h_n \vec{u}_n) = 0, \qquad (2.2\ \text{a,b})$$

where

$$B_n = \frac{1}{2}|\vec{u}_n|^2 + p_n / \rho, \qquad \zeta_n = \vec{k} \bullet \nabla \times \vec{u}_n$$

$$\vec{D}_n(\vec{u}_1, \vec{u}_2) = \left(\frac{\lambda_i}{h_n}\right)(\vec{u}_1 - \vec{u}_2)(-1)^n - \left(\frac{\lambda}{h_2}\right)\vec{u}_2\delta_{n2} + \frac{1}{h_n}(\nabla \bullet A h_n \nabla)\vec{u}_n \qquad (2.3\ \text{a,b})$$

where δ_{nm} is the Kronecker delta .

The equations are nearly the same as used in PINH. These are, in (2.2 a), the horizontal momentum equations for each layer. The stress appears as a body force in layer 1; that term is divided by the layer thickness since it is really a surface stress. The dissipation consists of the three terms given in (2.3 b). The first is an interfacial friction term whose coefficient is λ_i. It exerts and equal and opposite stress on each layer

proportional to the velocity difference. The second term is a bottom friction term proportional to λ again divided by the second layer thickness. The remaining term is our representation of lateral momentum mixing. We have used this model of interfacial friction to couple the two layers instead of a cross isopycnal velocity so that in the steady state we can represent the horizontal transport by a streamfunction since our equation for mass conservation (2.2b) has no cross isopycnal velocity. Thus, for *steady flows* (2.2 b) is identically satisfied by the representation in terms of the streamfunction ψ_n,

$$\vec{u}_n h_n = \hat{k} \times \nabla \psi_n, \quad n = 1,2 \tag{2.4}$$

where h_n are the actual thicknesses of the layers including the variations due to topography and the variations of the interface due to the motion. Indeed, for steady motions the momentum equations can be usefully written

$$q_n \nabla \psi_n = \nabla B_n - \frac{\vec{\tau}}{h_1}\delta_{n1} - \vec{D}_n(\vec{u}_1, \vec{u}_2) \tag{2.5}$$

The vorticity equation for the lower layer combined with the mass conservation equation for the layer yields the potential vorticity equation for layer 2 which for a steady state is,

$$\vec{u}_2 \bullet \nabla\left(\frac{\zeta_2 + f}{h_2}\right) = \frac{1}{h_2}\vec{k} \bullet \nabla \times \vec{D}_2 \tag{2.6}$$

so that for weak enough dissipation, we would anticipate the potential vorticity for layer 2 to be locally conserved. Furthermore, if there is a closed contour of potential vorticity, q_2, in the lower layer an integral of (2.5) around that contour implies that

$$\oint_{Cq_2} \vec{D}_2 \bullet \vec{t} ds = 0 \qquad (2.7)$$

This constraint holds for all nonlinearity but it will be most usefully employed in the linear theory of the next section where the contours of constant potential vorticity are the ambient isolines of $q_2 = f/h_2$ and h_2 is known.

3. Linear theory

To help establish a conceptual picture of the dynamics in the two-layer model it is useful to consider the situation when the wind stress is weak enough to produce a slow, laminar circulation in the upper layer. We will also examine the case where the dissipation is very weak. In particular, we will avoid regions in which the lateral mixing is important, i.e. we will remain outside lateral friction, i.e. Munk, layers whose thickness we can estimate as $\delta_M = \left(\frac{A}{\beta}\right)^{1/3}$ (although over regions of closed potential vorticity contours the thickness generally would be of the order of $\left(\frac{Ah_2}{\lambda}\right)^{1/2}$) and we consider the case where $\delta_M << x_T$, $\delta_M << r_T - r_I$.

The interfacial friction coefficient λ_i and the bottom friction coefficient λ are also taken as small i.e.

$$(\lambda, \lambda_i) / \beta h_2 << (x_T,\ r_T - r_I)\,. \qquad (3.1)$$

3a. The meridional island

We first consider the linear flow for the island oriented in the north-south direction as in Figure1. Topography is limited to the lower layer. For small dissipation the flow in the upper layer, outside of any western boundary layers, will be in Sverdrup balance as long as the flow in the lower layer is order one, or less, with respect to the Sverdrup flow. The solution for the Sverdrup flow in the upper layer is found for the four regions shown in Figure 2. The island in the figure is the circular island but the regional domains are the same with obvious changes for the meridional island.

In regions A, B, C the solution for the layer 1 stream function satisfies

$$\beta \psi_{1x} = \vec{k} \bullet curl \vec{\tau} = 2\tau_o / r_o \qquad (3.2)$$

for our wind stress given by (2.1). The Sverdrup solution for the upper layer is, in regions A, B, and C,

$$\psi_1 = \frac{2\tau_o}{\beta r_o}[x - x_e(y)],\ \ x_e(y) = \left(r_o^{\,2} - y^2\right)^{1/2} \qquad (3.3a)$$

whereas the solution to (3. 2) in region D, in the "beta shadow" west of the island, is

$$\psi_1 = \frac{2\tau_o}{\beta r_o} x + \Psi_{1I} \qquad (3.3b)$$

where the final term in (3.3b) Ψ_{1I} is the island constant for the upper layer island. The constant is determined by the usual Island Rule, e.g. PINH,

$$\Psi_{1I} = \frac{1}{(y_n - y_s)} \int_{y_s}^{y_n} \psi_{1sv}(0, y) dy - \oint_{C_I} \vec{\tau} \bullet d\vec{s} \qquad (3.4)$$

where the first term on the right hand side is the Sverdrup streamfunction (3.3a) evaluated on the island at $x = 0$ in the upper layer while the last term in (3.4) is the integral of the wind stress, tangent to the island, integrated around the island. If the island is very thin in the upper layer the second term is negligible for our constant curl wind. The island constant is calculated in Appendix A.

When the contours, C_{q2} , of f/h_2 are closed, i.e. when the topographic contribution to the potential vorticity in layer two is large enough, the constraint (2.7) applies on those contours (see 3.25 c below). Further, if the coefficients of bottom and interfacial friction satisfy (3.1) the constraint (2.7) implies

$$\lambda_i \oint_{C_{q2}} \frac{\nabla \psi_1 \bullet \vec{n}}{h_1 h_2} ds = (\lambda + \lambda_i) \oint_{C_{q2}} \frac{\nabla \psi_2 \bullet \vec{n}}{h_2^2} ds \qquad (3.5)$$

on each such contour and the potential vorticity equation implies in the linear limit that those isolines are given by the isolines of f/h_2 which are known *a priori*. The potential vorticity equation in turn implies that

$$\psi_2 = \Psi_2(q_2) \qquad (3.6)$$

or from (3.5)

$$\frac{d\Psi_2}{dq_2} = \frac{\lambda_i}{\lambda + \lambda_i} \frac{\oint_{C_{q2}} \frac{\nabla \psi_1}{h_1 h_2} \bullet \vec{n} ds}{\oint_{C_{q2}} \frac{\nabla q_2 \bullet \vec{n}}{h_2^{\,2}} ds} \qquad (3.7)$$

Note that this implies that for an order one streamfunction in the upper layer we can anticipate an order one flow in the lower layer on the closed contours. Instead, on the open q_2 contours the lower layer streamfunction will be $O(\lambda_i)$.

Over the topography on the long sides of the skirt

$$\nabla q_2 = \frac{-fs}{h_2^{\,2}} \left[\vec{i} - \vec{j} \frac{\beta h_2}{fs} \right], \quad s = \frac{h_T}{x_T} \qquad (3.8)$$

where s is the slope of the topography on the long, meridional, sides of the island. On the rounded tips of the island the slope is the same. The second term in the square bracket of (3.8) is numerically very small and is order $\beta x_T / f$. This has important consequence for the forcing.

The *outward* normals on the right and left hand sides of the island are

$$\vec{n}_R = \frac{\vec{i} - \vec{j} \beta h_2 \big/ fs}{\left(1 + \left[\frac{\beta h_2}{fs} \right]^2 \right)^{1/2}}, \quad \vec{n}_L = \frac{-\vec{i} - \vec{j} \beta h_2 \big/ fs}{\left(1 + \left[\frac{\beta h_2}{fs} \right]^2 \right)^{1/2}} \qquad (3.9\ \text{a,b})$$

and note that $h_2 / f = q_2$ and so is constant along a pv contour.

On the right hand side of the island

$$\nabla q_2 \bullet \vec{n}_R = -\frac{fs}{{h_2}^2}\left\{1+\left(\frac{\beta}{q_2 s}\right)^2\right\}^{1/2} \tag{3.10}$$

and using the fact that on that contour $ds = dy\left\{1+\left(\frac{\beta}{q_2 s}\right)^2\right\}^{1/2}$ we find that the portion of

the integral in the denominator of (3.7) on the right hands side of the island is:

$$\int_{y_s}^{y_n} \frac{\nabla q_2 \bullet \vec{n}_R}{{h_2}^2} ds = -{q_2}^4 \frac{s}{\beta} \int_{y_s}^{y_n} \frac{\beta}{f^3} dy \left\{1+\left(\frac{\beta}{q_2 s}\right)^2\right\} \tag{3.11}$$

where we have ignored the relatively small $O(x_T / y_n)$ contributions from the island tips.

The integral on the left hand side yields the same result so, ignoring only the northern and

southern tips of the island the denominator in (3.7) yields

$$\oint_{C_{q2}} \frac{\nabla q_2 \bullet \vec{n}}{{h_2}^2} ds = -{q_2}^4 \frac{s}{\beta}\left(\frac{{f_n}^2 - {f_s}^2}{{f_n}^2 {f_s}^2}\right)\left\{1+\left(\frac{\beta}{q_2 s}\right)^2\right\} \tag{3.12}$$

Note that the last term in the curly bracket,

$$\left(\frac{\beta}{q_2 s}\right)^2 = O\left(\frac{\beta h_2 x_T}{f h_T}\right)^2 = O\left(\frac{\beta x_T}{f}\right)^2 << 1 \tag{3.13}$$

is negligible.

There are three contributions to the integral in the numerator of (3.7). There is, first of all, the contribution from the Sverdrup solution along the pv contours that are nearly meridionally oriented on each side of the skirt.

This term in the numerator in (3.7) can be easily calculated on the long sides of the topography since

$$\nabla\psi_1 = \frac{2\tau_o}{\beta r_o}\left[\hat{i} + \hat{j}\frac{y}{\left(r_o^2 - y^2\right)^{1/2}}\right], \quad x > 0$$

while for $x < 0$

(3.14 a,b)

$$\nabla\psi_1 = \frac{2\tau_o}{\beta r_o}\hat{i}$$

The largest term of the forcing, $\nabla\psi_1 \bullet \vec{n}$, consists of the meridional flow proportional to $\frac{\partial\psi_1}{\partial x}$ multiplied by the x component of the normal vector. Since this yields a forcing that is the same on both sides of the island it will cancel when integrated around the contour.

This will leave only the term $\frac{\partial\psi_1}{\partial y}$ multiplied by the very tiny component of the normal in the meridional direction. Similarly, the jump in the Sverdrup solution across the boundary between region D and regions A and C represent narrow, zonally oriented boundary layers whose flow contributes only due to the inner product of the ψ_2 gradient

in the *y* direction with the small component of the normal in that direction and it too is very small. For the record and for the sake of comparison with the more effective forcing from the topographic tips of the island we present here the result of those calculations without showing the details. The sum of these first two contributions is, when combined with (3.11)

$$\frac{d\psi_2}{dq_2} = \frac{\lambda_i}{\lambda+\lambda_i}\frac{2\tau_o}{H_1}\frac{\beta}{s^2}q_2^{-4}\left[\frac{I_b}{f_o}+\frac{1}{2}\left\{\left(1-\frac{y_n^{\,2}}{r_o^{\,2}}\right)^{1/2}-\frac{r_o}{y_n}\sin^{-1}\left(\frac{y_n}{r_o}\right)\right\}\frac{f_n-f_s}{f_nf_s}\right]\frac{f_n^{\,2}f_s^{\,2}}{f_n^{\,2}-f_s^{\,2}} \quad (3.15)$$

where the integral

$$I_b = \int_{\eta_s}^{\eta_n}\frac{1}{(1+b\eta)}\frac{\eta}{\left(1-\eta^2\right)^{1/2}}d\eta, \quad \eta = y/r_o \qquad (3.16)$$

where $f = f_o(1+b\eta), \quad b = \dfrac{\beta r_o}{f_o}$ and the integral as a function of b is shown in Figure 3. It is negative and for small b it is numerically small. The remaining term in the square bracket in (3.15) comes from the calculation of the zonal boundary layers, modeled as delta function jumps in the upper layer streamfunction. Note that for $y_n / r_o < 1$ the two terms cancel to order $\left(\dfrac{y_n}{r_o}\right)^2$ so (3.15) is even smaller than its coefficient implies. In fact the principal contributions to (3.7) come from the two, relatively small semi-circular tips of the topography at the extreme northern and southern ends of the skirt. With the same Sverdrup solution we can calculate these contributions to the numerator of (3.7).

We introduce a local radial coordinate system whose origin is at $(0,\ y_n)$ so that

$$r = \left(x^2 + [y - y_n]^2\right)^{1/2}, \quad 0 \le r \le x_T \tag{3.17}$$

For the relatively small range of y in this semicircular domain the potential vorticity contours are nearly coincident with the bathymetry and hence are lines of constant r. Indeed, since in this region,

$$h_2 = H_2 + \frac{h_T}{x_T}(r - x_T) \tag{3.18a}$$

it follows that r can be written in terms of q_2,

$$r = x_T + \left(\frac{f_n}{q_2} - H_2\right)\frac{x_T}{h_T} \tag{3.18b}$$

The unit normal to the lines of constant r is simply

$$\vec{n} = \hat{i}\cos\theta + \hat{j}\sin\theta \tag{3.19}$$

The inner product of $\nabla\psi_1$ with the normal will give two terms. The first of which is proportional to $\cos\theta$ and will integrate to zero on the arc between 0 and π. The remaining term is again the inner product with the y component of the normal which is now order one so that

$$\int_0^{\pi} \frac{\nabla\psi_1 \bullet \vec{n}}{H_1 h_2} r d\theta = \frac{2\tau_o}{\beta r_o H_1}\frac{q_2}{f_n}\int_0^{\pi} r d\theta \frac{y\sin\theta}{\left[r_o^{\,2} - y^2\right]^{1/2}} \tag{3.20}$$

Since in this region $y = y_n + r\sin\theta$ and since r is less than or equal to x_T we can approximate (3.20) by replacing y everywhere in (3. 20) by y_n so that the contribution to the numerator in (3.7) is simply

$$\int_0^{\pi} \frac{\nabla\psi_1 \bullet \vec{n}}{H_1 h_2} r d\theta = \frac{2\tau_o}{\beta r_o H_1} \frac{q_2}{f_n} \frac{2y_n x_T}{\left[r_o^2 - y^2\right]^{1/2}} \left\{1 + \frac{f_n}{q_2 h_T} - \frac{H_2}{h_T}\right\} \qquad (3.21)$$

where the final bracket in (3.21) is the representation of r/x_T.

A similar analysis at the southern end of the island on its semi-circular tip yields a similar result and when the two of them are added together they provide the *dominant* contribution to (3.7), namely,

$$\frac{d\Psi_2}{dq_2} = \left(\frac{\lambda_i}{\lambda_i + \lambda}\right)\left\{\frac{-4\tau_o}{sH_1 r_o}\right\} \frac{y_n x_T}{\left(r_o^2 - y_n^2\right)^{1/2}} \frac{f_n f_s^2}{\left(f_n^2 - f_s^2\right)} \bullet$$
$$\bullet\left[\frac{1}{q_2^3}\left(1 + \frac{f_n}{f_s}\right)\left(1 - \frac{H_2}{h_T}\right) + \frac{1}{q_2^4}\frac{2f_n}{h_T}\right] \qquad (3.22)$$

Comparing (3.22)with the contributions from the other two sources given by (3.15) shows that the ratio of this contribution to the former is of the order

$f_o s x_T / h_2 \beta r_o = O\left(\frac{h_T}{h_2}\frac{f_o}{\beta r_o}\right)$. As long as the ratio h_T/h_2 is order one, it shows that the forcing from the tips is of the order of $f_o / \beta r_o$. (In fact, as we show below, that ratio has to be order one in order to obtain closed contours at all.) In our ocean basin this parameter is about an order of magnitude greater than one. It is therefore reasonable, at

first order in this parameter, to neglect all forcing in this geometry *except the forcing at the two extreme ends of the island's skirt*. This was a result that was surprising to us but it seems to also agree fairly well with the numerical evidence described below.

We can now integrate (3.22) and use the condition that the lower layer streamfunction vanishes on the outer closed contour where $q_2 = f_n / H_2$ leading to our final result,

$$\psi_2 = A\left[\frac{1}{2s}\left(1+\frac{f_n}{f_s}\right)\left(1-\frac{H_2}{h_T}\right)[1-\frac{f_n^{\,2}}{q_2^{\,2}H_2^{\,2}}]+\frac{2}{3s}\frac{H_2}{h_T}\left(1-\frac{f_n^{\,3}}{q_2^{\,3}H_2^{\,3}}\right)\right] \qquad (3.23)$$

where, recall, $s = h_T / x_T$

$$A = \left(\frac{\lambda_i}{\lambda_i+\lambda}\right)\left\{\frac{-4\tau_o}{H_1 r_o}\right\}\frac{y_n x_T}{\left(r_o^{\,2}-y_n^{\,2}\right)^{1/2}}\frac{f_s^{\,2}}{\left(f_n^{\,2}-f_s^{\,2}\right)}\frac{H_2^{\,2}}{f_n} \qquad (3.24)$$

Figure 4 shows the form of the streamfunction ψ_2 over the skirt at the mid latitude, $y = 0$ when the height of the skirt at the island is half the layer depth, i.e. when $h_T = 0.5H_2$ and when $h_T = 0.999H_2$. More precisely, the figure shows ψ_2 divided by the coefficient *A*.

The calculation is shown for an anticyclonic wind stress curl. The circulation in the lower layer is anticyclonic. Note that the abscissa is x/x_T and falls a bit short of unity. This is because of the slope of the q_2 contours in the *x*.*y* plane due to the β effect. This leaves a small sliver of the edge of the skirt outside the closed q_2 contours. The weak

solution over the flat region can be continued on the *open* pv contours over this sliver but for concision we will not discuss it in detail. When the maximum height of the skirt almost reaches the interface between the layers the form of the stream function profile is different and is flatter in the neighborhood of the island with strong variations of ψ_2 limited to the outermost closed potential vorticity contours nearer the edge of the skirt. This follows directly from (3.23). In this case the flow is reduced over the inner part of the skirt and expelled to the outermost q_2 contours.

The remarkable feature of the lower layer flow in this geometry is how a very localized region of strong forcing can produce a circulation on the closed potential vorticity contours that essentially shoots a substantial flow all around the entire island. While logical, it is certainly non intuitive.

The dependence of the circulation in the lower layer on the steepness of the topography is a subtle one. As (3.24) shows, the flow along the potential vorticity contours is reduced when *s* the skirt slope is increased. On the other hand if the slope is too small the potential vorticity contours, rather than girdling the island, strike the island and are blocked so the *domain* of closed contours is reduced as *s* is reduced. Indeed, the outermost closed contour, starting a $x = x_T$ and $y = y_n$ satisfies the relation

$$\frac{f_n}{H_2} = \frac{f}{H_2 - h_T(1 - x/x_T)} \qquad \text{(3.25 a, b)}$$

$$\Rightarrow \quad \frac{x}{x_T} = 1 - \frac{H_2}{h_T}\left(1 - \frac{f}{f_n}\right)$$

so that the condition that it reach the southern boundary without striking the island at x = 0, is simply

$$\frac{h_T}{H_2} > \frac{\beta(y_n - y_s)}{f_n} \qquad (3.25c)$$

For an island of length 1400km and for $\beta = 2\ 10^{-11}$ m/s and $f = 10^{-4}$ sec^{-1}, this yields a critical value of h_T / H_2 of 0.28. Topography lower than this will have all the potential vorticity contours blocked and the $O(1)$ motion, with respect to the friction parameters satisfying (3.1) will be expunged. Thus small slopes have no region of geostrophically resonant flow while large slopes have broader regions of geostrophically resonant flow but those flows have an streamfunction that decreases with increasing slope (3.24). Nevertheless, the local volume flux, which is the gradient of ψ_2, will involve the derivative of the depth, canceling the factor of s in the denominator of (3.24) leading to the prediction that the local mass flux will be independent of the *slope* although it will still depend on the local, varying depth h_2.

If the topography is steep enough to intrude into the upper layer the situation becomes much more complex. However, in the region of the upper layer with steep topography and closed pv contours in the *upper* layer the flow on the closed contours is essentially barotropic and, as predicted in PINH, the flow is much stronger, $O(\lambda^{-1})$. A full treatment of that problem is beyond the scope of the present paper. However, the important qualitative point is that the presence of stratification has shielded the lower layer from the direct effect of the wind forcing. The circulation on the closed q_2 contours

is smaller than in the barotropic case although still much larger than in the flat region of the lower layer.

3b. The circular island

In view of the weak projection of the forcing on the contour of integration we have turned to another island geometry, shown in Figure 2. The skirt provides a topographic potential vorticity gradient in the lower layer that is in the radial direction. Indeed, in the lower layer,

$$\nabla q_2 = \frac{-1}{h_2}\left[\frac{f}{h_2} s\hat{r} - \beta\hat{j}\right], \qquad (3.26a)$$

where $\hat{r}$ is the unit radial vector and $\hat{j}$ is a unit vector in the *y* direction. As before, *s* is the slope on the skirt , here $r_I \le r \le r_T$ and *s* is now given by

$$s = h_T / (r_T - r_I) \qquad (3.26b)$$

The magnitude of the second term in (3.26a) compared to the first is very small, of the order of 10^{-2} and we will neglect this in what follows to simplify the calculation, i.e. we are neglecting the β effect in the *lower layer* over the topography. Had we done this for the meridional island we would be left with no forcing except from the tips. For the circular island an $O(1)$ term remains and we are justified in neglecting small terms in

β over the topography. In this sense the circular island is very similar to the meridional island except that it is all "tip". Again, (3.7) is the essential equation. To calculate the numerator in (3.7) we must be aware of the regions with different Sverdrup solutions. In regions A, B, and C in Figure 2 the solution is again,

$$\psi_1 = \frac{2\tau_o}{\beta r_o}(x - x_e(y)), \quad x_e(y) = \left(r_o^{\,2} - y^2\right)^{1/2} \text{ in A,B, C} \qquad (3.27a)$$

Now, however, in the beta shadow to the west of the island, region D, the solution is

$$\psi_1 = \frac{2\tau_o}{\beta r_o}(x - x_w(y)) + \Psi_{1I}, \quad x_w = -\left(r_I^{\,2} - y^2\right)^{1/2} \qquad (3.27b)$$

where the curved boundary introduces a new feature to the solution in the region. We will also need the island constant Ψ_{1I} and that calculation is given in Appendix A. The result is

$$\Psi_{I1} = \frac{2\tau_o}{\beta r_o}\left[-\frac{1}{2}\left(r_o^{\,2} - r_I^{\,2}\right)^{1/2} - \frac{\pi}{4}r_I - \frac{1}{2}\frac{r_o^{\,2}}{r_I}\sin^{-1}\left(\frac{r_I}{r_o}\right)\right] \qquad (3.28)$$

With the neglect of the beta effect in the calculation of (3.7) the contour of integration is just any circle between the island and the outer radius, r_T , of the skirt. Because of the north-south symmetry of the integrands when the relatively small beta effect is ignored we can carry out the integral in (3.7) on any circle of radius *r* between the angles of 0 and π. In starting from the *x* axis to the east of the island the integral proceeds counter

clockwise until the contour intersects the boundary between regions A and D. This occurs at an angle $\pi - \theta_s$ where, as seen in Figure 5,

$$\theta_S = \sin^{-1}(r_I / r) \tag{3.29}$$

where the solution for ψ_1 in the integrand must be abruptly changed. Note that as $r \to r_I$ θ_S approaches $\pi/2$. We will do the integrand in pieces and take into account the delta function-like behavior of ψ_1 in addition. Since $\hat{r} = \hat{i}\cos\theta + \hat{j}\sin\theta$, where θ is the azimuth angle, we have in region A

$$\nabla\psi_1 \bullet \vec{n} = \frac{2\tau_o}{\beta r_o}\left[\cos\theta + \frac{y\sin\theta}{\left(r_o^{\,2} - y^2\right)^{1/2}}\right] \tag{3.30a}$$

while in region D

$$\nabla\psi_1 \bullet \vec{n} = \frac{2\tau_o}{\beta r_o}\left[\cos\theta - \frac{y\sin\theta}{\left(r_I^{\,2} - y^2\right)^{1/2}}\right] \tag{3.30b}$$

Note that the second term in (3. 30b) may become very large and it is certainly greater than the equivalent term in (3.30a). In distinction to the meridional island the circular island's western coast is curved and introduces a new, relatively large term to the forcing. This is similar to the aforementioned case if the *eastern* boundary of the basin is convex facing westward rather than concave as for the circular basin. For the same curl the convex boundary of the western portion of the island acts the same way changing the sign

of the zonal Sverdrup flow. The nature of the flow in the basin is a powerful function of the *shape* of the basin perimeter since in Sverdrup dynamics that information is propagated in a non dispersive manner westward.

In calculating the integrals needed in (3.7) we can use the fact that $y = r\sin\theta$ and that r itself can be written as a function of q_2 using the relation between the thickness of the lower layer, namely,

$$r = r_T - \frac{\Delta r}{h_T}\left[H_2 - \frac{f_o}{q_2}\right], \quad \Delta r = r_T - r_I \tag{3.31}$$

After a small calculation we obtain

$$\frac{\oint_{Cq_2} \frac{\nabla\psi_1 \bullet \vec{n}}{h_1 h_2} ds}{\frac{2\tau_o}{f_o \beta r_o H_1}} =$$

$$q_2 r\left[2\int_0^{\pi-\theta_S} \frac{\sin^2\theta}{\left[m^2 - \sin^2\theta\right]} d\theta - 2\int_{\pi-\theta_S}^{\pi} \frac{\sin^2\theta}{\left[n^2 - \sin^2\theta\right]} d\theta;\right] \tag{3.32}$$

$$n = r_I / r; \quad m = r_o / r, \quad \theta_S = \sin^{-1}(r_I / r)$$

The factor of 2 in each integral results from using only half of the total range of integration and using the symmetry in y when the beta effect is ignored over the skirt. The two integrals in (3.32) yield terms of opposite signs. This is very much like the

situation referred to earlier where there is a change in sign of forcing if the eastern boundary of the *basin* is convex rather than concave facing west. Here the term of opposite sign is introduced by the island geometry itself. As a short hand we will call the two integrals in the square bracket of (3.32) I_m and I_n with obvious definitions. The calculation is incomplete until we consider the effect of the abrupt jump in the solution across the boundary between regions A and D as we did for the meridional island.

Consider now the jump in the Sverdrup streamfunction across the line $y = r_I$. That jump in the y direction is

$$\psi_{1A} - \psi_{1D} = -\frac{2\tau_o}{\beta r_o}\left\{\left(r_o^{\,2} - r_I^{\,2}\right)^{1/2}\right\} - \Psi_{1I} \qquad (3.33)$$

That means that that in evaluating $\nabla\psi_1 \bullet \vec{n}$ in the upper layer we will again approximate the gradient as a delta function, namely in the neighborhood of $y = r_I$

$$\nabla\psi_1 = -\vec{j}\left(\frac{2\tau_o}{\beta r_o}\left\{\left(r_o^{\,2} - r_I^{\,2}\right)^{1/2}\right\} + \Psi_{1I}\right)\delta(y - r_I) \qquad (3.34a)$$

so that

$$\nabla\psi_1 \bullet \vec{n} = -\left[\frac{2\tau_o}{\beta r_o}\left\{\left(r_o^{\,2} - r_I^{\,2}\right)^{1/2}\right\} + \Psi_{1I}\right]\sin\theta_S\,\delta(y - r_I); \quad \theta = \pi - \theta_S \qquad (3.34b)$$

Note that θ_S is positive. In (3.34b) r is the circle on which the integral in (3.7) is being carried out. Now, our integral is an integral at fixed r and so ds is $rd\theta$. To evaluate the integral using the delta function we need to use the relation, for constant r, $rd\theta = dy/\cos\theta$. Keeping in mind that the integral in (3.7) is in the counterclockwise sense, it means that as an integral in y the segment in the immediate neighborhood of $y = r_I$ is

$$\int \frac{\nabla\psi_1 \bullet \vec{n}}{h_1 h_2} ds = \frac{-q_2}{H_1 f_o} \int_{r_{I+}}^{r_{I-}} \left[\frac{2\tau_o}{\beta r_o} \left[r_o^{\,2} - r_I^{\,2} \right]^{1/2} + \Psi_{1I} \right] \frac{\sin\theta}{\cos\theta} \delta(y - r_I) dy$$

$$= \frac{q_2}{H_1 f_o} \tan\theta \left[\frac{2\tau_o}{\beta r_o} \left[r_o^{\,2} - r_I^{\,2} \right]^{1/2} + \Psi_{1I} \right] \tag{3.35}$$

which, when combined with (3.28) yields

$$\int \frac{\nabla\psi_1 \bullet \vec{n}}{h_1 h_2} ds = -\frac{q_2}{H_1 f_o} \tan(\theta_s) \frac{2\tau_o}{\beta r_o} 2 \left(\frac{1}{2} [r_o^{\,2} - r_I^{\,2}]^{1/2} - \frac{1}{2} \frac{r_o^{\,2}}{r_I} \sin^{-1}(r_I / r_o) - \frac{\pi r_I}{4} \right) \tag{3.36}$$

as the contribution of both the northern and southern jumps in the streamfunction to the forcing of the lower layer flow. For small r_I / r_o the first two terms in the final bracket in (3.36) nearly cancel, the residual being of order $-\frac{2}{3}\frac{r_I^{\,2}}{r_o}$ which would be much smaller than the last term in the bracket so that the contribution is dominated by the portion of the island constant related to the circulation of the stress around the upper layer island. In fact, for very large r_o, the variation of the distance from the island to the eastern

boundary, over the latitude range of the island is negligible and the eastern boundary act as if it were straight contributing little to the integral (3.32) and (3.36).

When the contribution (3.36) is included in (3.32) we finally obtain

$$\frac{d\psi_2}{dq_2} =$$
$$-\frac{\lambda_i}{\lambda+\lambda_i}\frac{2\tau_o}{s\beta H_1 r_o}\frac{{f_o}^2}{2\pi {q_2}^3}\left[I_m - I_n - \frac{1}{r}\tan(\theta_S)\left([{r_o}^2 - {r_I}^2]^{1/2} - \frac{{r_o}^2}{r_I}\sin^{-1}(r_I / r_o) - \frac{\pi r_I}{2} \right)\right] \quad (3.37)$$
$$s = h_T / (r_T - r_I)$$

Once $\frac{d\psi_2}{dq_2}$ is calculated the azimuthal transport around the pv contours in the lower layer is obtained by multiplying (3.37) by $\frac{dq_2}{dr}$, where

$$\frac{dq_2}{dr_2} = -\frac{f_o}{{h_2}^2}s \quad (3.38)$$

Figure 6 shows the form of the azimuthal transport $\partial\psi_2 / \partial r$ for an island for which $r_I / r_T = 0.5$ and $r_o / r_T = 5$ and for which the wind stress has a constant *negative* curl. The figure shows that the flow is everywhere anticyclonic. If we had ignored the contribution from the zonal boundary layers we would have obtained *cyclonic* circulation over part of the range in *r* as a consequence of the forcing on the western curved boundary of the island (the integral I_n) It is important to recall that a major part of the forcing, due to the equal meridional flow on both sides of the island cancels in the contour integral leaving

the residuals related to the curvature of the boundaries to determine the balance of forcing on the contours of potential vorticity. We can imagine that viscous effects and the no-slip condition will significantly alter the flow for radii very near the island, where in Figure 6 there is strong anticyclonic flow but the region beyond that should be external to such effects. Figure 6 also shows a calculation for which the ratio of the basin radius to the skirt radius is smaller i.e. r_o / r_T =2. This enhances the effect of the integral I_m and the flow is more strongly anticyclonic everywhere.

The other important attribute of the circular geometry can be seen from (3.32), i.e. that the derivative $d\Psi_2 / dq_2$ goes inversely with the slope *s*. Since the azimuthal transport on the closed q_2 contours is this function times the potential vorticity gradient, which goes like the slope of the skirt, the transport is again, as in the meridional island, *independent of the size of the slope*.

Note that using (3.37) and (3.38) the ratio of the transport in the lower layer to the Sverdrup transport in the upper layer is

$$\frac{v_2 h_2}{v_1 h_1} = O\left(\frac{\lambda_i}{\lambda_i + \lambda} \frac{h_2}{H_1} \frac{[\text{bracket}]}{2\pi} \right) \qquad (3.39)$$

where [bracket] refers to the square bracket in (3.37) which is plotted in Figures 7 for $r_o / r_T = 2$ and is order one or less except near the inner boundary where the tangent term becomes large and the result, based on our delta function representation of the boundary layer contribution, becomes unreliable. Thus we anticipate the flow to be somewhat smaller in the lower layer than in the upper layer although of the same order. For a

barotropic model, as in PINH, the flow on closed q_2 contours would go as λ^{-1}, so as in the case of the meridional island, the principal effect of the stratification is to shield the lower layer from the direct forcing of the wind and reduce the response of the topographic resonance.

Given the delicacy of the relative balances of the *residuals* of the upper layer forcing on the lower layer it is important to compare these idealized linear results with numerical calculations which include the effects of lateral friction and nonlinearity.

4. Numerical model and results for the linear regime

The previous theoretical results indicate that deep circulations can be driven along topography that encircles an island through a fairly simple parameterization of coupling with the upper layer wind-driven flow. The circulation along a closed contour of potential vorticity results from a delicate balance between forcing from the upper layer and dissipation, in the form of bottom drag, interfacial stress, or horizontal viscosity. Owing to the symmetries in the problem, the net forcing on the deep layer is much weaker than the wind forcing in the upper layer, yet the mean circulation can be of similar strength. Numerous assumptions are required in order to make the problem analytically tractable and, while each are defensible, an independent confirmation of the result is desirable. In this section, the basic circulation patterns and parameter dependencies predicted by the theory are tested using a numerical model. The model contains more complete physics, and so

provides an inherent validation of the analytic result, while the theory provides a clear interpretation of the balances that determine the mean circulation.

The numerical model used in this study is based on the Miami Isopycnal Coordinate Ocean Model (MICOM, Bleck et al. 1992). The model solves the primitive equations of motion using an isopycnal vertical coordinate. The MICOM solves prognostic equations for the isopycnal-layer averaged horizontal momentum, layer thickness (and sea surface height), temperature, and salinity. We have made several simplifications for the present problem. Temperature and salinity are uniform within each layer, and so the model effectively uses only the potential density field. There is no mixing of density (or tracers) between isopycnal layers and there is no surface buoyancy flux, so the model is adiabatic. All calculations reported here use two isopycnal layers.

The initial layer thicknesses are 1000 m for both the upper and lower layers, giving a maximum total depth of 2000 m. The horizontal grid spacing is 10 km for the meridional island cases and since we found more sensitivity to horizontal resolution for the circular island calculations we used 5 km for the circular island cases. The Coriolis parameter varies linearly with latitude as $f = f_0 + \beta y$, where $f_0 = 0.75 \times 10^{-4} s^{-1}$ and $\beta = 2\ x\ 10^{-13}$ cm^{-1} s^{-1}, and $y = 0$ at the mid-latitude of the basin. The change in density between the two layers is 2.81Kg m^{-3}, resulting in a baroclinic deformation radius of 50 km.

The upper layer is forced by a body-force representation of wind stress, as in (2.2a) with a uniform wind stress curl. The deep layer is forced through an interfacial stress term that is proportional to the difference between the upper layer velocity and the lower

layer velocity, as in the linear theory (2.3b). Viscous dissipation is represented as a lateral Laplacian friction.

The relative strengths of the model forcing and dissipation are characterized by several boundary layer thicknesses. The strength of the wind stress is specified indirectly through the inertial boundary layer thickness, $\delta_I = \left(\frac{\tau_o}{2 r_o H_1 \beta^2} \right)^{1/2}$. The strength of dissipation is specified through the previously defined frictional Munk boundary layer thickness.

For comparison with the linear theory, we choose relatively weak forcing so that the relative vorticity of the mean flow remains small and the large-scale mean circulation is stable to baroclinic and barotropic instabilities. The inertial boundary layer thickness for the meridional island cases is $\delta_I = 5$ km, while the Munk layer thickness $\delta_M = 20$ km (A = 160 m^2 s^{-1}), giving a ratio $\delta_I / \delta_M = 0.25$. For the circular island calculations, $\delta_I = 2$ km, while the Munk layer thickness $\delta_M = 10$ km (A = 20 m^2 s^{-1}), giving a ratio $\delta_I / \delta_M = 0.2$. The model calculations are started from rest and run for a period of 20 years, at which point the fields are essentially steady.

a) meridional island

Here we present numerical results for thin meridional islands in a circular basin, and compare them with the predictions of the linear theory previously developed. To further clarify the expected dependencies of the lower layer transport over the skirt on the geometrical parameters, we show in Figure 8 a map obtained from (3.23), evaluated at

the mid latitude. The map gives the transport as a function of the basin radius r_o and of the island half-length y_n, for a fixed value of the topography "aspect ratio", $x_T / y_n = 0.5$. Qualitatively similar maps are obtained for higher (lower) values of the aspect ratio, with higher (lower) values of the transports, respectively. For fixed r_o, the transport increases monotonically with y_n mostly because of the increasing dependence on x_T in (3.23), while for given island length it decreases when going to larger basins, so that maximum transport is obtained near the right lower corner of the map. These qualitative dependencies are confirmed by the numerical simulations, even though the corresponding transport values are generally lower than those obtained from (3.23). In the following, we will restrict to a basin of 1000 km of radius, unless otherwise indicated.

A typical steady state obtained in the simulations is that of Figure 9, showing the streamfunctions of the two layers for a configuration with an island of 800 km, surrounded by a 250 km wide skirt that reaches 600 m of height. The forcing is from a constant curl wind stress, whose size is determined by the non-dimensional parameters previously specified, that are appropriate for a linear context. The solution in the upper layer is very close to what may be expected on the basis of the barotropic linear theory developed in Pedlosky et al. 1997, with almost coinciding numerical and theoretical values of the island constant Ψ_I (0.483 Sv and 0.486 Sv, respectively). This indicates that the interfacial drag coupling with the lower layer is small enough not to affect the upper layer dynamics (see the next subsection for a more detailed analysis of the effects of the interfacial drag on the circulation). On the other hand, the same coupling drives significant circulations in the lower layer, one of which is confined in the region of the western boundary layer, while the other, over the skirt, is characterized by streamlines

that closely follow the PV contours encircling the island. Much weaker flow is observed over the rest of the flat bottom region. This picture is in qualitative agreement with the theory, although the transport around the island of 1.64 x 10^{-3} Sv is more than four times smaller than the one predicted by (3.23). In this case, the theoretical transport value could be brought somewhat closer to the numerical one by including the contributions of the tip regions to the integral in the denominator of (3.7), which are of order of $x_T / y_n = 0.625$. However, the discrepancy in the transport values is systematic, suggesting that effects not included in the analytic model, such as that of lateral friction, play a role in slowing down the flow over the skirt.

An interesting point emerging from the analytic calculation of Section 3a is the observation that the main contributions to the transport appears to come from the regions of the skirt tips, which prompted us to retain only these contributions in the derivation of (3.23). The simulations confirm this behavior. Two runs with the same geometry and parameters of Figure 9, but different island lengths (y_n = 200 km, and y_n = 600 km), yield transports over the skirt of 1.46 x 10^{-3} Sv, and 2.01 x 10^{-3} Sv, respectively, indicating a weak dependence of the transport on the island length, and supporting the idea that the forcing along the lateral portions of the PV contours is less effective than the one acting in the tip regions. This is further clarified in Figure 10, where we plot the integrand in the numerator of (3.7), $\nabla\psi_1 \bullet \vec{n} / h_2$, over the skirt region, as computed from the upper layer numerical solution of Figure 9, with some PV contours superimposed (dashed lines). The forcing is weak and cyclonic to the west of the island, and of the same order of the anticyclonic forcing present in the outer part of the eastern skirt. On the other hand, strong, localized anticyclonic regions are present to the northeast and southeast of

the island tips, that provide a major driving source for the circulation around the island, as suggested by the analytic estimates. However, the picture emerging from the simulation is more complex, since near the eastern side of the island there is also an intense forcing pattern due to the presence of a boundary layer, whose effects could not be included in the analytic approach.

Another point to be explored is the dependence of the transport on the skirt height. Figure 11 shows that this dependence, for the geometry of Fig. 9, is quite weak; the transport is somewhat lower for smaller and larger skirt heights, peaking around a height of 500 m. The analytic dependence (not shown) is even weaker, with the transport approximately constant above 500 m of height. This means that the s^{-1} dependence in the coefficient *A* in (3.23) gets partly overridden by the more complex one of the term in brackets. The same weak dependence of transport on skirt height was found for other configurations, and we anticipate a similar behavior for the circular island case.

b) circular island

The mean circulation for a circular island in a circular basin is shown in Figure 12. The island radius $r_I = 250$ km, the topographic skirt radius is $r_T = 500$ km, and the basin radius $r_0 = 1000$ km, giving $r_i / r_T = 0.5$ and $r_0 / r_T = 2$. The skirt height is 500 m, giving a topographic slope $s = 0.002$. The streamfunction in each layer is nondimensionalized by the theoretical island constant (3.28).

The circulation in the upper layer reflects the Sverdrup transport away from the island, with the flow direction in regions A, B, and C tracing the shape of the eastern boundary. To the west of the island the zonal flow changes sign because the island west

coast is convex, as expected from the linear theory. There is also a strong boundary layer along the eastern side of the island, which is required because the island constant is greater than the Sverdrup transport between the island and the eastern boundary, see (3.28). This eastern boundary layer was not included in the theory, but the westward boundary layers extending from the northern and southern tips of the island, also evident in the figure, were included. The influence of this eastern boundary layer is to drive an anticyclonic circulation within approximately δ_M of the island. This region close to the island is also where the theory predicts a very strong anticyclonic circulation driven by the northern and southern tip boundary layers. Because of the neglect of dissipation and this western boundary layer in the theory, we do not expect quantitative agreement between the model and theory close to the island.

The model produces a mean anticyclonic circulation around the island of strength $0.023\ \Psi_{I1}$. This transport is carried over a width of O(200 km), while the upper layer transport of ψ_1 is carried over O(1000 km) width, so the ratio of their transports per unit width is approximately 0.1. This is in general agreement with the theoretical prediction (3.39). The transport around the island is more than 2 orders of magnitude greater than the deep transport over the flat bottom, as expected from the theory, and confirms that even relatively weak coupling between the upper and deep layer can force an O(1) flow over the closed topographic contours. There is a significant north-south asymmetry in the streamfunction because the potential vorticity contours do not coincide with topographic contours because of the influence of β. This contribution was neglected over the topographic skirt in the theory, and the numerical result demonstrates that its

primary influence is to distort the circulation slightly but it does not change the qualitative response in the deep layer.

The primary purpose of the model is to verify the basic balances predicted by the theory. Rather than carry out a detailed comparison between model and theory, it is perhaps more useful to test that the parameter dependencies predicted by the theory are reproduced by the model. Expression (3.37) indicates that, for $\lambda = 0$, the deep circulation over the skirt should be independent of λ_i. The circulation over the flat bottom is much weaker than the circulation over the skirt, but is expected to increase linearly with λ_i. A series of model calculations have been carried out in which the coupling coefficient has been varied, while all other parameters are the same as for the above standard case. The circulation strength over the skirt is shown as a function of the coupling coefficient in Fig 13a. The recirculation varies with the coupling strength approximately as $\left(\lambda_i / \beta h_2 \left(r_T - r_I\right)\right)^{1/2}$. Recall that the theory assumes that this ratio is much less than 1. The model requires lateral viscosity for computational stability and, as a result, we are not able to find a regime in which the solution is independent of the coupling strength. We can anticipate this general behavior from the theory (3.39), as dissipation (represented by λ in the theory) will cause a decreasing recirculation strength with decreasing λ_i. The boundary layer width $\left(Ah_2 / \lambda_i\right)^{1/2}$ is 20 km for $\left(\lambda_i / \beta h_2 \left(r_T - r_I\right)\right) = 10^{-2}$, but increases to O(300 km) for the weakest coupling strength in Fig. 13a. This viscous dissipation was not included in the theory, and for dissipation values required for computational stability

in the numerical model ($A = 20$ m^2 s^{-1}) as we move into the regime of small λ_i, the boundary layer becomes important.

The transport over the flat interior, between the topography and the eastern boundary, is always less than that over the topographic skirt, but it shows a stronger dependence (nearly linear) on the coupling coefficient. This result is consistent with the theory, and confirms that the dynamics over the region of closed potential vorticity contours are very different from that found in the region of blocked potential vorticity contours. Even for weak coupling in the presence of lateral dissipation the circulation over the closed topographic contours is much stronger than over the flat interior. The specific parameter dependence in Fig. 13a is difficult to predict analytically, but the overall result, that the resonant circulation over the topography is intermediate to that for the barotropic flow and the flat interior, is robust to the details of the model physics.

A second prediction from the theory is that the transport over the skirt should be independent of the bottom slope s, because $d\psi_2 / dq_2$ depends on s^{-1}, while dq_2 / dr depends linearly on s. The slope was varied in a series of calculations by changing the height of the topographic skirt while keeping the width constant at 250 km (Fig. 2b). The circulation over the topography is only weakly dependent on bottom slope for $s > .8 \times 10^{-3}$, which corresponds to heights greater than 200 m. For bottom slopes weaker than this the planetary vorticity gradient is sufficiently strong compared to topographic beta that the region of closed potential vorticity contours is eliminated. There is a more gradual decrease in the circulation strength for steep bottom slopes. This is consistent with the expectation from the theory, as discussed in

Section 3 where for stronger slopes the circulation becomes influenced by the change in the total depth and its role in decreasing the circulation consistent with (3.23) which qualitatively applies also to the circular island case.

5. Nonlinear numerical results

The linear calculations in the preceding sections parameterized forcing of the deep ocean through a simple interfacial stress between the upper layer and the deep layer. This approach is intended to represent the tendency, in baroclinic fluids, for momentum to be transmitted from the upper ocean to the deep ocean as a result of baroclinic instability or vertical mixing. The advantage of such an idealized approach is that it allows for closed form analytic solutions and a straightforward interpretation of the driving mechanisms for the deep ocean.

It is, however, a drastic simplification of what is likely in the real ocean to be a much more complex process. Given the apparent sensitivity of the linear model to details of the forcing, it is important to confirm that the basic result remains relevant in more nonlinear regimes representative of the real ocean.

We have carried out a number of numerical model calculations in configurations similar to those already discussed, but with sufficiently strong forcing of the upper layer that the circulation becomes unstable and strongly time-dependent. The interfacial stress used for the linear calculations has been removed, and the only forcing on the deep layer comes from the resolved time-dependent motions. We report results from one of these calculations (although all have been found to produce qualitatively similar results) to demonstrate the basic response predicted by the simple linear models is also produced in

a nonlinear model.

A calculation with a narrow meridional island, as in Section 4a, has been carried out with 5 km horizontal resolution and forcing and dissipation characterized by an inertial boundary layer thickness of 15 km (wind stress 70 times stronger than for the linear calculations) and a Munk boundary layer thickness of 10 km. The stratification has been reduced so that the baroclinic deformation radius is 30 km and the large-scale flow is more susceptible to baroclinic instability. The model was started at rest and integrated for a period of 20 years.

The mean streamfunction over the final 5 years of integration in the upper and lower layers is shown in Fig. 14. The upper layer circulation to the east of the island largely reflects the expected Sverdrup flow, but there are considerable differences in the vicinity of and to the west of the island. The model produces strong, barotropic recirculation gyres on the offshore side of the western boundary current.

The flow in the western shadow of the island is similar to what one would expect from Sverdrup theory, however near the southern portion over the bottom topography, the flow turns to the north. There is a small closed anticyclonic recirculation near the northern tip of the island in the upper layer which we found in most nonlinear calculations .

The deep layer is dominated by closed recirculations near the western boundary and around the skirt topography. The circulation around the island is approximately the same as the island constant in the upper layer, stronger than predicted by the linear theory but of the same order of magnitude as the upper layer wind-driven circulation. The flow around the island is strongly baroclinic, particularly along the western flank where the

deep flow is in the opposite direction to the local wind-driven flow.

The nonlinear model result is very complex and includes processes not considered in the linear theory (such as loss of momentum from the upper layer to the deep layer and eddy-driven recirculation gyres). A detailed analysis of this regime is beyond the scope of the present study. It is encouraging, however, that the primary prediction from the linear theory, that the combined effect of closed f/h_2 contours in the deep layer and stratification produce deep recirculations of the same order as the upper layer wind-driven flow, is reproduced in this model that explicitly resolves the time-dependent forcing of the deep layer through instabilities of the upper layer flow.

6. Discussion and conclusions

The addition of both topography and baroclinicity to the dynamics of flow around planetary scale islands produces new and important qualitative changes in the circulation. The presence of baroclinicity, represented in our model by our two layer system, introduces for the first time the issue of the vertical structure of the flow.

The presence of topography in the barotropic model in PINH introduced closed geostrophic contours around the island and the resulting flow, directly wind driven, could be very large since the geostrophic resonance on those contours led to velocities bounded only by the dissipation experienced by the flow on each closed contour. Most of that flow remained trapped to the topography and the Island Rule, which focused primarily on the interchange of flow between ocean basins on each side of the island, could be simply reinterpreted by applying it to the region defined by the outermost closed geostrophic contour instead of the island's surface boundary.

In the two layer model, the flow in the lower layer is not directly forced by the wind but is instead forced by the action of the upper layer on the lower layer. In our linear models of section 3, for example, the drag on the lower layer by the upper layer flow depends on the coupling constant λ_i between the layers. When the coupling is weak, as seems realistic, the flow in the lower layer on the closed contours never exceeds the flow in the upper layer and, in linear theory, is reasonably independent of the value of the coupling as long as it is small. This is in contrast to the flat region outside the topographic skirt where the resulting lower layer flow is very weak and order λ_i itself. Our numerical modeling of this linear regime shows a weak dependence on λ_i over the topography, possibly as the result of lateral friction neglected in the theory and does show the linear dependence of the flat interior on λ_i. Thus the baroclinic model predicts a deep flow with a strength intermediate between the flow on the skirt in the barotropic model and the flow in the deep interior where there are no closed potential vorticity contours. In that sense the presence of closed potential vorticity contours provided by the topography allows a locally efficient mechanism to transfer momentum to the lower layer.

Furthermore, since the flow in the deeper layer is driven by the velocity of the upper layer Sverdrup flow rather than the wind stress itself, portions of that driving are ineffective in driving the flow. In particular, the meridional flow in our constant wind stress curl forcing is equal on each side of the island and cancels in the contour integral around the island that determines the net forcing that drives the deep response. This leads to a surprisingly sensitive dependence of the deep flow on the geometry of the island as well as the geometry of the basin. For example, in the case of the long, meridionally oriented island, the major driving comes from the upper layer flow acting on the

relatively small northern and southern rounded tips of the island's topography. That localized forcing is responsible for the major impetus for motion over the entire length of the potential vorticity isolines in the lower layer. The forcing on the rest of the island's perimeter, although locally as strong, is almost completely self-canceling so that the total forcing is dominated by the effects of the tips. For the circular island the forcing is everywhere stronger but the convex shape of the western boundary of the island produces a local forcing that would actually drive a flow in the opposite direction to that imposed by the sense of the wind stress curl were it not for the contributions to the forcing of the zonally oriented boundary layers produced, in turn, by the discontinuities of the Sverdrup solution in the region west of the island. At the same time the forcing on the eastern side of the island depends on the curvature of the basin boundary and when that curvature is weak (on the meridional scale of the island), or non existent (in the case of a straight eastern boundary) there is no forcing provided by the eastern edge of the island. Thus the nature of the response to the wind forcing is a rather complex function of the basin and island geometry.

The strength of the circulation has a complex dependence on the magnitude of the slope. If the slope is too small the presence of the planetary vorticity gradient allows the potential vorticity contours to strike the island's boundary instead of encircling it and the resulting deep circulation will be very weak. On the other hand, for moderately strong slopes the transport streamfunction is inversely proportional to the slope. However, the local mass flux in the deep layer along the potential vorticity contours is independent of the slope. We have noted that for very large slope there is a decline in the flux, a dependence predicted by the analytical theory and confirmed numerically.

The effects of lateral friction are neglected in the analytical theory of section 3. Yet, the numerical experiments in the linear limit show no sign of baroclinic instability in the basin interior removed from the skirt and boundary currents. That implies that there is sufficient damping, due to lateral friction to expunge the growth rate of instabilities since the meridional flow should be unstable at all levels of shear if inviscid. That, in turn implies an intrinsic Reynolds number of order one on the deformation radius scale. The presence of this irreducible level of friction may contribute to the quantitative differences between inviscid theory and numerical experiment.

If the island were large enough and if the curl varied substantially in the zonal direction across the breadth of the island an additional forcing would arise which we have not considered in this study.

Most of our numerical studies of the same models have been restricted to rather weak forcing in order to compare with the linear, analytic theory developed here. Preliminary results of a more non linear nature exhibit qualitatively similar enhanced circulation on the closed f/h_2 contours of the lower layer topography indicating a preferential pathway for the vertical transmission of momentum downward in that region.

Acknowledgements : This research was supported in part by a grant from the National Science Foundation (JP) NSF OCE 0925061 and (MAS) NSF OCE 0926656.
We are delighted to be able to contribute to the volume honoring Professor Vladimir Kamenkovich for his lifetime of accomplishments in developing our understanding of the general circulation of the oceans

APPENDIX A

The Island Constant

It is shown in PINH that the island constant for single layer of fluid of constant depth, which will apply to the upper layer of our model in the linear limit is given by the following integrals

$$\Psi_{1I} = \frac{1}{(y_n - y_s)} \int_{y_s}^{y_n} \psi_{Sverdrup}(x_+(y), y)dy - \oint_{C_I} \frac{\vec{\tau} \bullet \vec{t}}{\beta(y_n - y_s)} ds \qquad \text{(A.1)}$$

The first term on the right hand side is the integral in y of the Sverdrup streamfunction evaluated on the eastern boundary of the island.

Meridional island of section 3a

The Sverdrup streamfunction for the thin, meridional island on its eastern side is, from (3.3 a)

$$\psi_1(0, y) = -\frac{2\tau_o}{\beta r_o}\left(r_o^2 - y^2\right)^{1/2} \qquad \text{(A.2)}$$

so that doing the integral in (A.1) leads us to

$$\Psi_{1I} = \frac{-2\tau_o}{\beta r_o}\left[\frac{1}{2}\left(r_o^2 - y_n^2\right)^{1/2} + \frac{r_o^2}{2y_n}\sin^{-1}\left(\frac{y_n}{r_o}\right)\right] \qquad \text{(A.3)}$$

for the case where $y_s = -y_n$ as in our model.

The circular island of section 3b

For the solution (3.27b) the eastern boundary of the island boundary is $x_+ = \left(r_I^2 - y^2\right)^{1/2}$. Thus the first integral is

$$\frac{1}{(y_n - y_s)} \int_{y_s}^{y_n} \frac{2\tau_o}{\beta r_o} \left[\left(r_I^{\,2} - y^2 \right)^{1/2} - \left(r_o^{\,2} - y^2 \right)^{1/2} \right] dy, \quad y_n = -y_s = r_I$$

$$= \frac{2\tau_o}{\beta r_o} \left[\frac{r_I \pi}{4} - \frac{1}{2} \left(r_o^{\,2} - r_I^{\,2} \right)^{1/2} - \frac{r_o^{\,2}}{2 r_I} \sin^{-1}(r_I / r_o) \right] \tag{A.4}$$

while the second term is easily calculated using Stokes theorem for the constant curl wind stress of our model and that term is just $-\frac{2\tau_o}{\beta r_o}$, which when combined with (A.4) yields (3.38).

REFERENCES

Bleck, R.C., D. Hu, and L.T. Smith, 1992. Salinity-driven thermocline transients in a wind-driven and thermohanine-forced isopycnal coordinate model of the North Atlantic. J. Phys. Ocean., *22*, 1486-1505.

Godfrey, J. S. 1989. A Sverdrup model of the depth-integrated flow from the world ocean allowing for island circulations. Geophys. Astrophys. Fluid Dyn. *45*, 89-112.

Pedlosky, J. 2010. Baroclinic flow around planetary islands in a double gyre; A mechanism for cross-gyre flow. J. Phys. Ocean. *40*, 1075- 1086.

Pedlosky, J. , L. J. Pratt, M.A. Spall, and K. R. Helfrich. 1997. J. Mar. Res. *55*, 1199-1251.

Pedlosky, J., R. Iacono, E. Napolitano and K. R. Helfrich. 2009. The skirted island: The effect of topography on the flow around planetary scale islands. J. Mar. Res. *67*, 435-478.

Spall, M.A. 2000. Buoyancy forced circulations around island and ridges. J. Mar. Res. *58*, 957-982

FIGURE CAPTIONS

Figure 1 a) The two layer model showing the topography and layer thicknesses for the meridionally oriented island. b) The depth contours in units of 1,000 meters. c) The isolines of potential vorticity f/h_2 in the lower layer.

Figure 2 The four regions for the upper layer Sverdrup solution. For the meridional island the inner circle is replaced by a north-south line.

Figure 3 The integral $I_b(b)$ for different y_n/r_O.

Figure 4 The form of the lower layer stream function as a function of x at the mid latitude, $y = 0$, for $h_T = 0.5H_2$ and $h_T = 0.999H_2$.

Figure 5 The outer circle is the contour of integration. The inner circle is the island in the upper layer. The angle θ_S is the critical angle for the integration in section 3b.

Figure 6 The azimuthal transport $\partial\psi_2 / \partial r$ obtained from (3.28) and (3.29) for $r_I / r_T =$ 0.5 and $r_o / r_T = 5$ and 2.

Figure 7 The square bracket in (3.37) for $r_o / r_T = 2$.

Figure 8 Maximum of the lower layer stream function over the skirt, as a function of the island half-length y_n and of the basin radius r_0, for h_T = 600 m and $x_T/y_n = 0.5$. The contour interval is 0.002 Sv.

Figure 9 Steady state stream functions for the two layers (upper layer above), from a simulation with an island of 800 km, surrounded by a skirt of 250km , 600 m tall, whose boundary is indicated by the dashed contour. The contour intervals are 0.05 Sv and 2.5 x 10^{-4} Sv, respectively. The lower layer pattern displays a closed circulation around the island, over the skirt, with streamlines closely following the contours of constant potential vorticity.

Figure 10 The integrand in the numerator of (3.7), measuring the strength of the forcing exerted by the upper layer, wind-driven dynamics, on the lower layer circulation. Equally spaced contours, with the solid (dotted) lines corresponding to anticyclonic (cyclonic) forcing, with the dashed lines indicating contours of constant potential vorticity.

Figure 11 The dependence of the transport on the topographic height h_T for the meridional island

Figure 12 Mean streamfunction for a) upper layer and b) lower layer for δ_M = 10 km, δ_I = 2 km, $\lambda_I = 10^{-5}$ m s^{-1}, r_I = 250 km, r_T = 500 km, and r_O = 1000 km. The streamfunction in both layers has been nondimensionalized by the upper layer island constant Ψ_I = .095 Sv, and the contour interval in a) is 0.1 and in b) is .004. The topography is indicated on a) by the gray circular contours, contour interval 200 m.

Figure 13 a) The total nondimensional transport over the topographic skirt (asterisks) and flat interior east of the topography (circles) as a function of the scaled coupling coefficient $\lambda_i / \beta h_2 (r_T - r_I)$. The straight lines have slopes proportional to $\lambda_i^{1/2}$ for the island result and λ_i for the interior result. b) The nondimensional transport over the skirt as a function of the bottom slope; the vertical dashed line is the approximate value for which the closed potential vorticity contours vanish.

Figure 14 Mean a) upper and b) lower layer streamfunction from the final 5 years of a 20 year integration for the nonlinear numerical model. The streamfunction in both layers has been nondimensionalized by the upper layer island constant. The contour interval is 0.25. The bottom topography is indicated in a) by the gray contours, contour interval 200 m.

a)

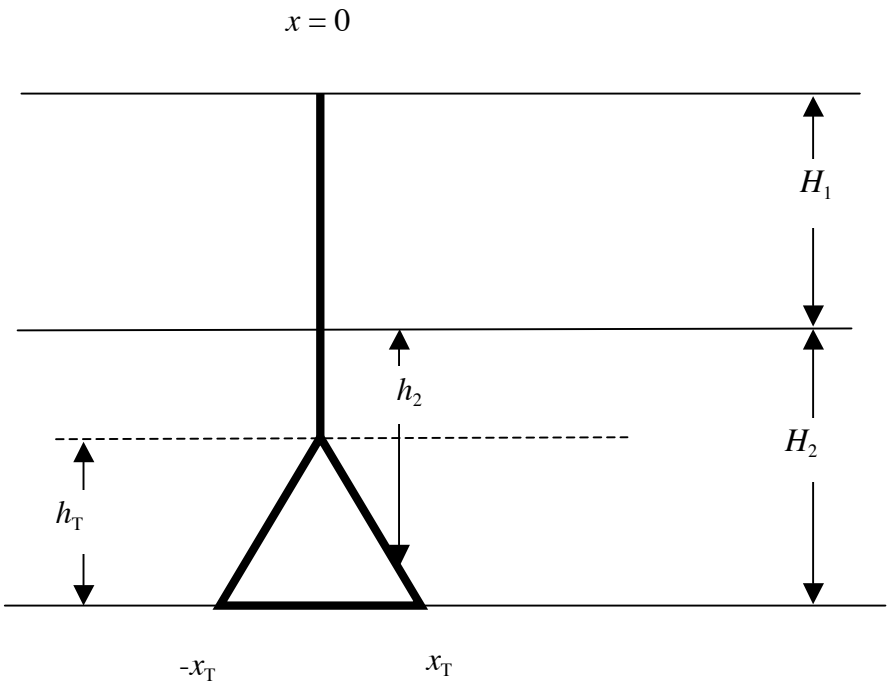
$x = 0$
H_1
h_2
H_2
h_T
$-x_T$
x_T

b)

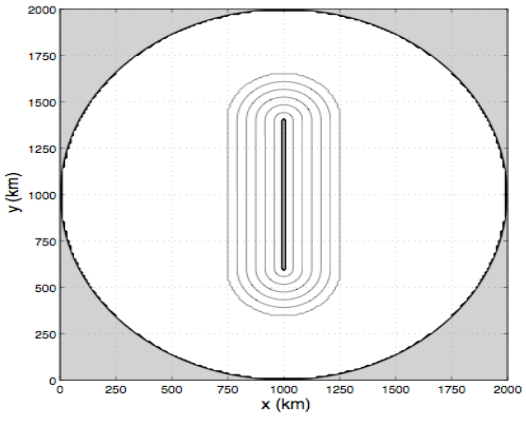
2000
1750
1500
1250
1000
750
500
250
0
y (km)
0
250
500
750
1000
1250
1500
1750
2000
x (km)

c)

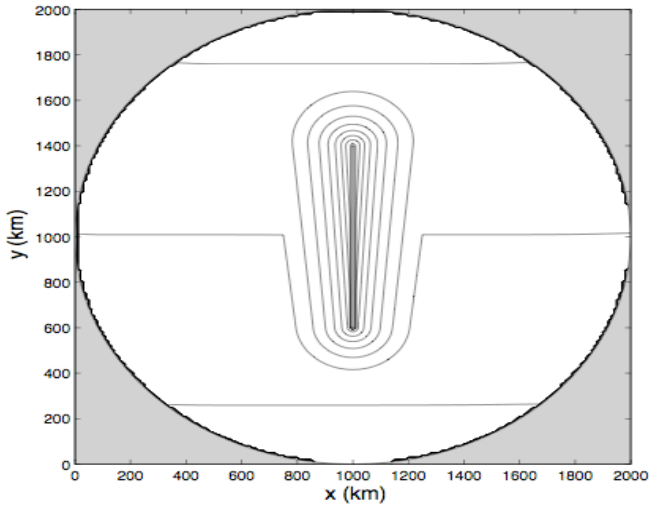

Figure 1 a) The two layer model showing the topography and layer thicknesses for the meridionally oriented island. b) The depth contours in units of 1,000 meters. c) The isolines of potential vorticity f/h_2 in the lower layer.

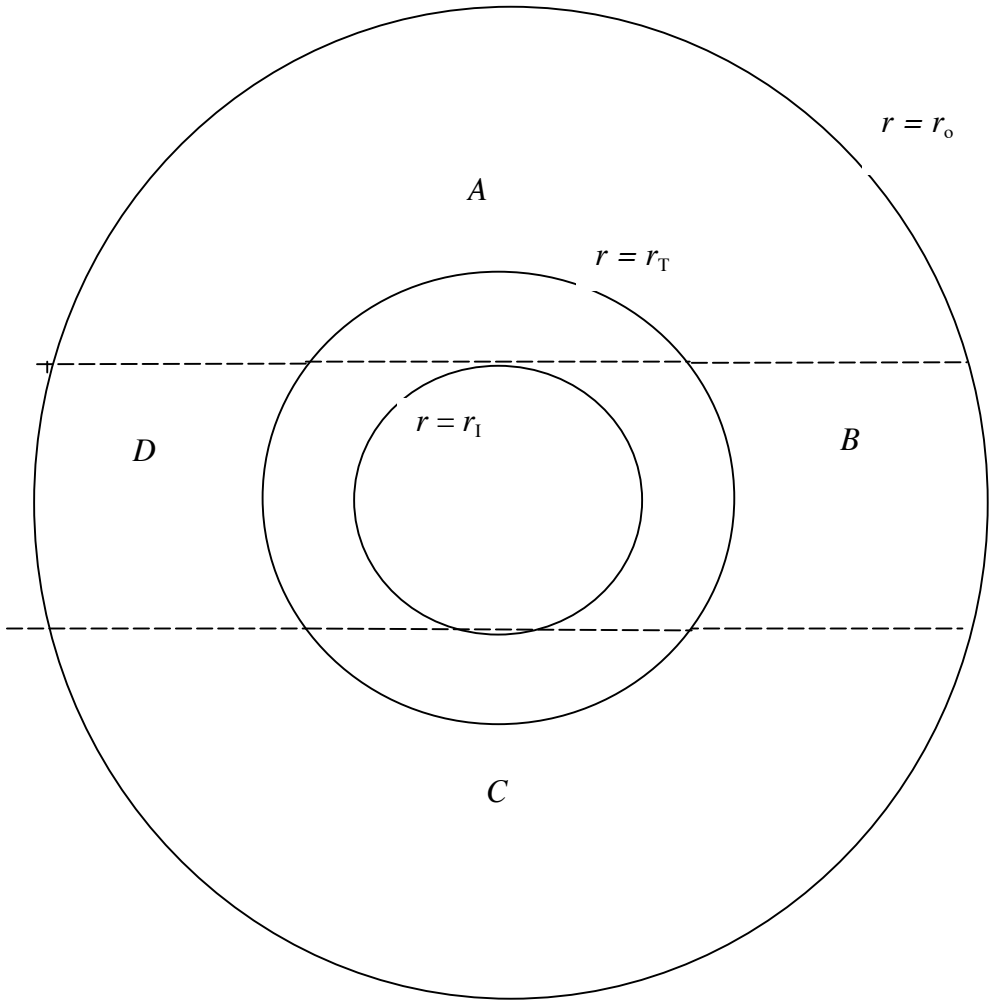

Figure 2 The four regions for the upper layer Sverdrup solution showing the island with inner radius r_I in the upper layer and the skirt in the lower layer extending to r_T. For the meridional island the inner circle is replaced by a north-south line.

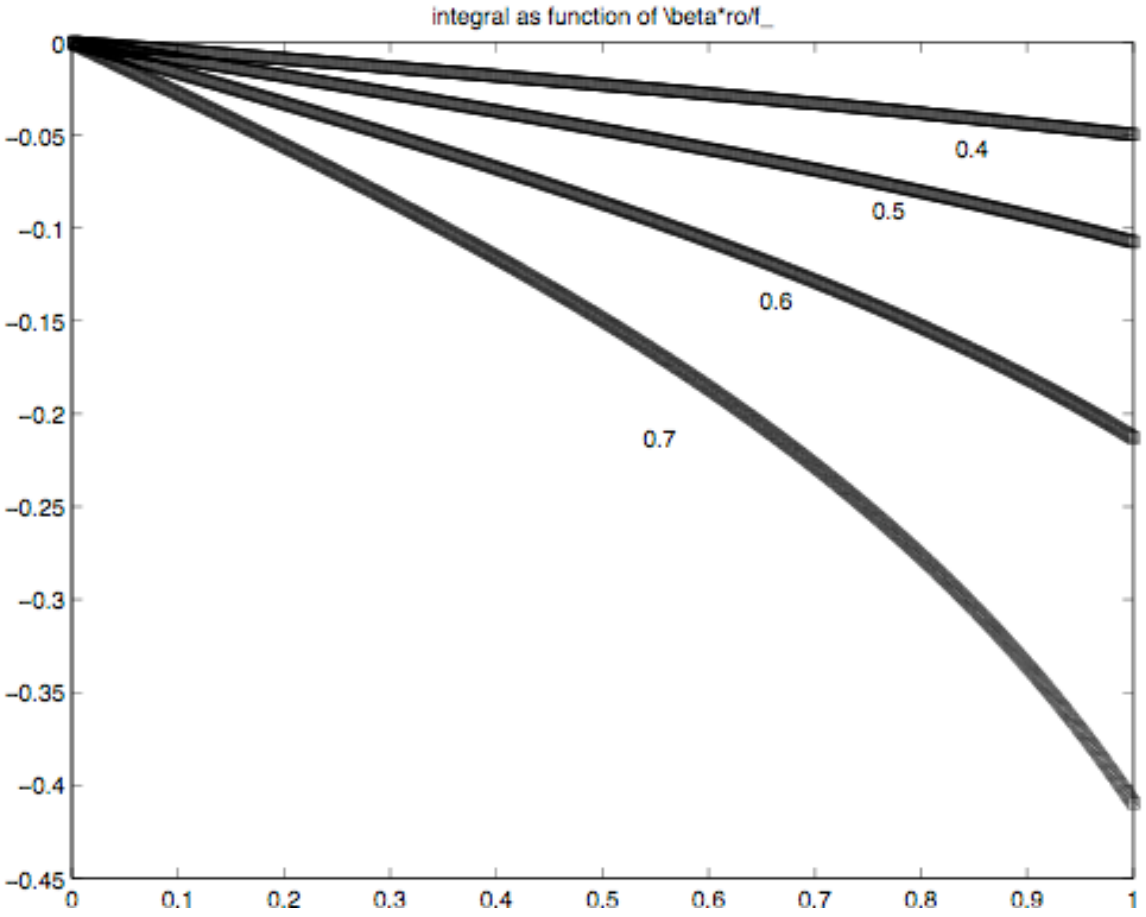

Figure 3 The integral $I_b(b)$ for different y_n/r_O.

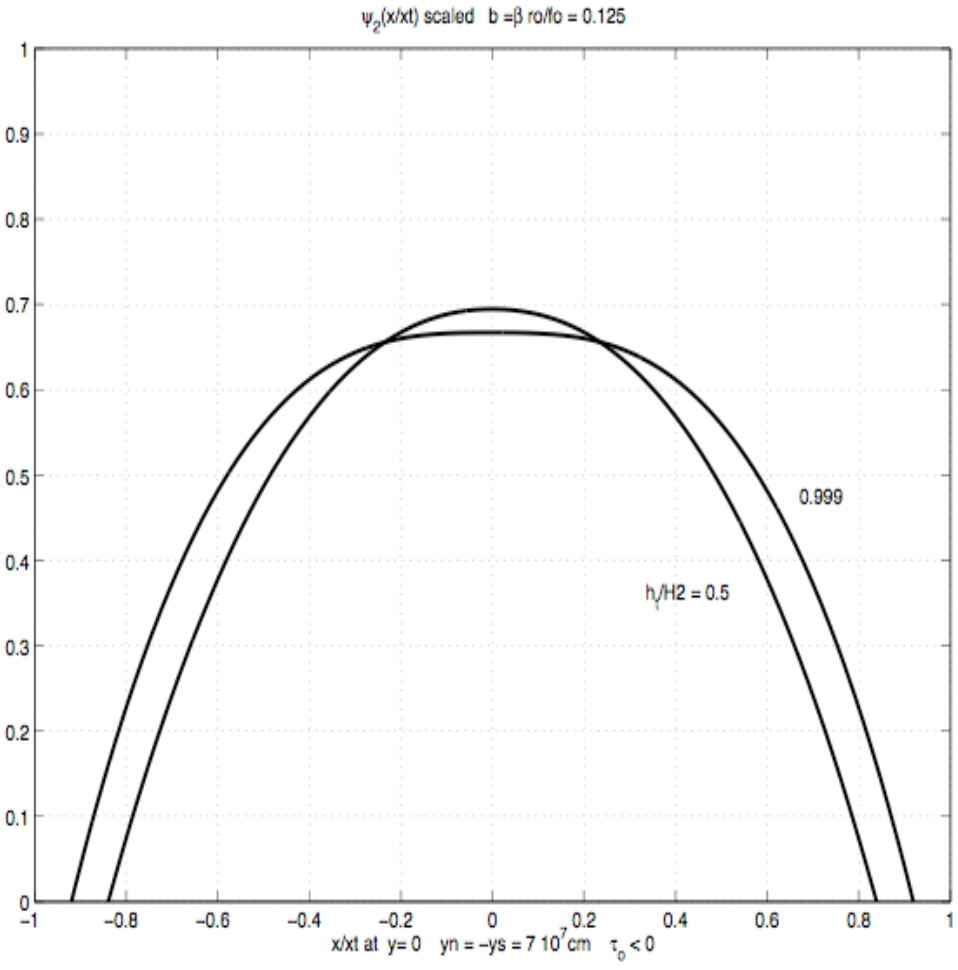

Figure 4 The form of the lower layer stream function as a function of x at the mid latitude, $y = 0$, for $h_T = 0.5H_2$ and $h_T = 0.999H_2$.

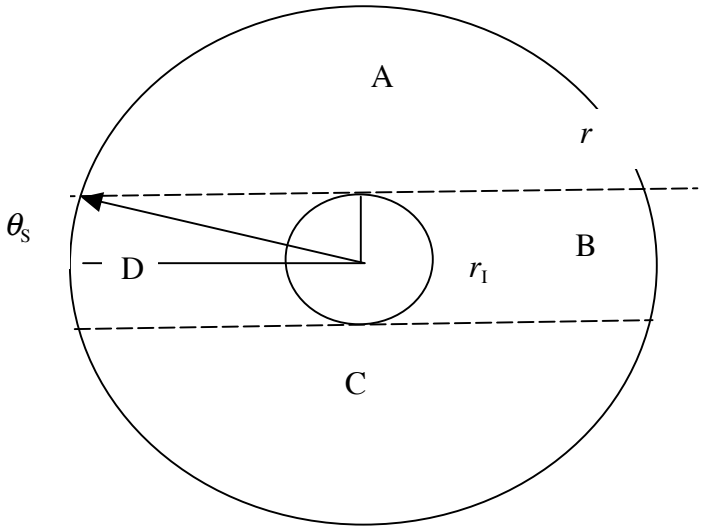

Figure 5 The outer circle is the contour of integration. The inner circle is the island in the upper layer. The angle θ_S is the critical angle for the integration in section 3b.

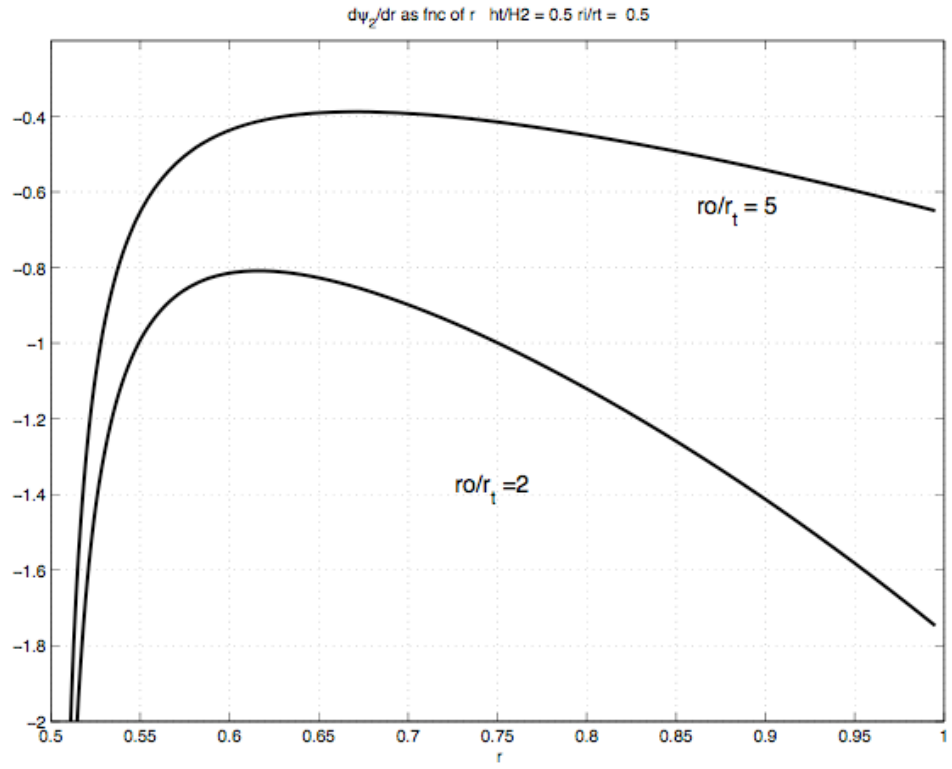

Figure 6 The azimuthal transport $\partial\psi_2 / \partial r$ obtained from (3.28) and (3.29) for r_I / r_T = 0.5 and r_o / r_T = 5 and 2.

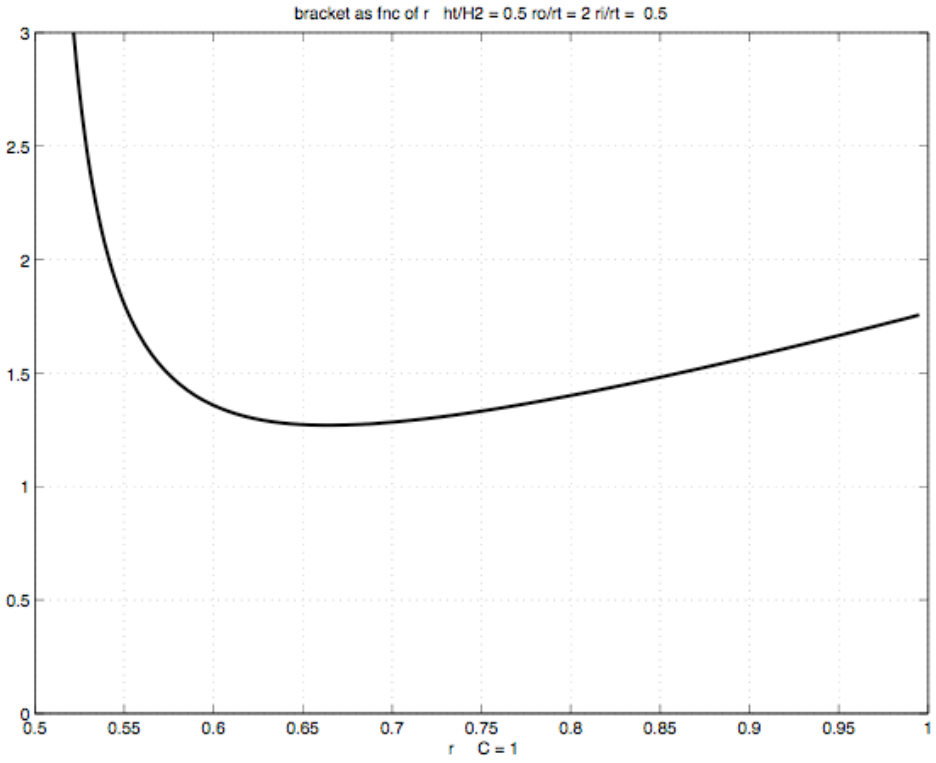

Figure 7 The square bracket in (3.37) for $r_o / r_T = 2$.

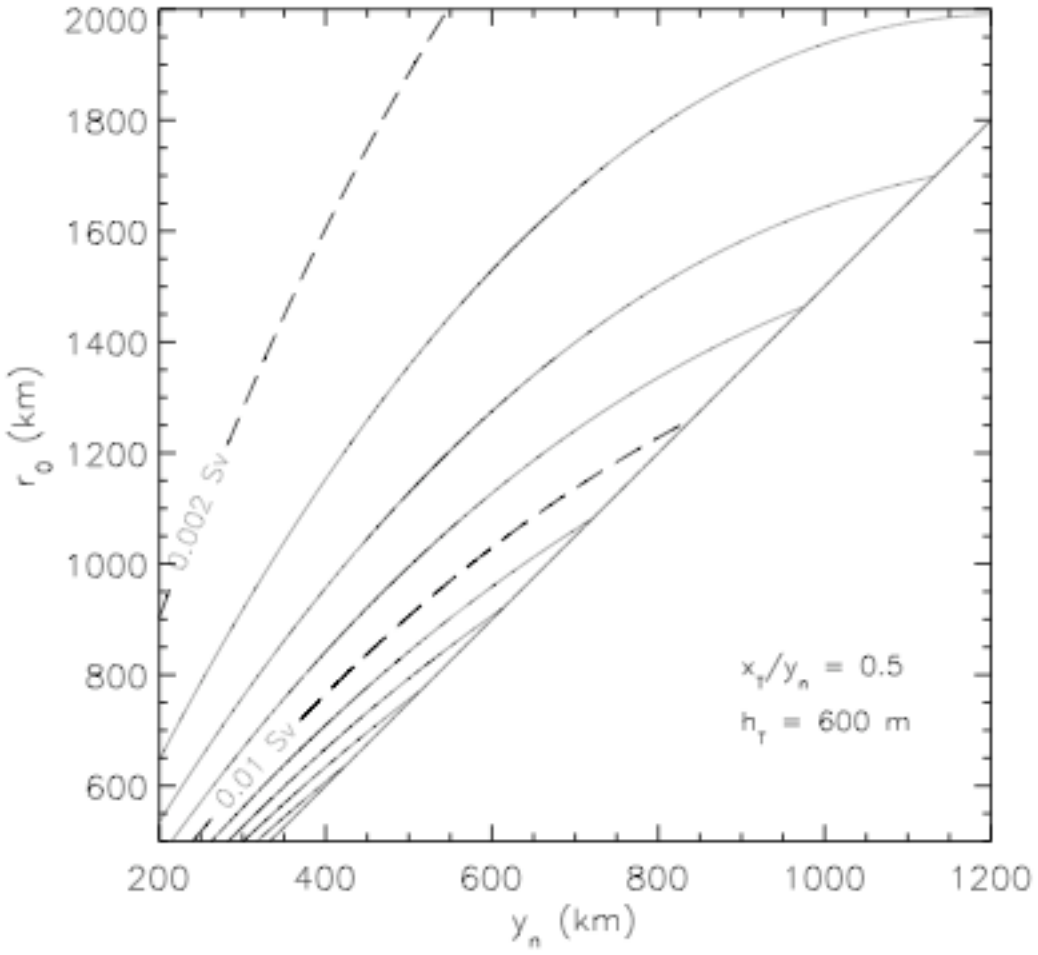

Figure 8 Maximum of the lower layer stream function over the skirt, as a function of the island half-length y_n and of the basin radius r_0, for h_T = 600 m and $x_T/y_n = 0.5$. The contour interval is 0.002 Sv.

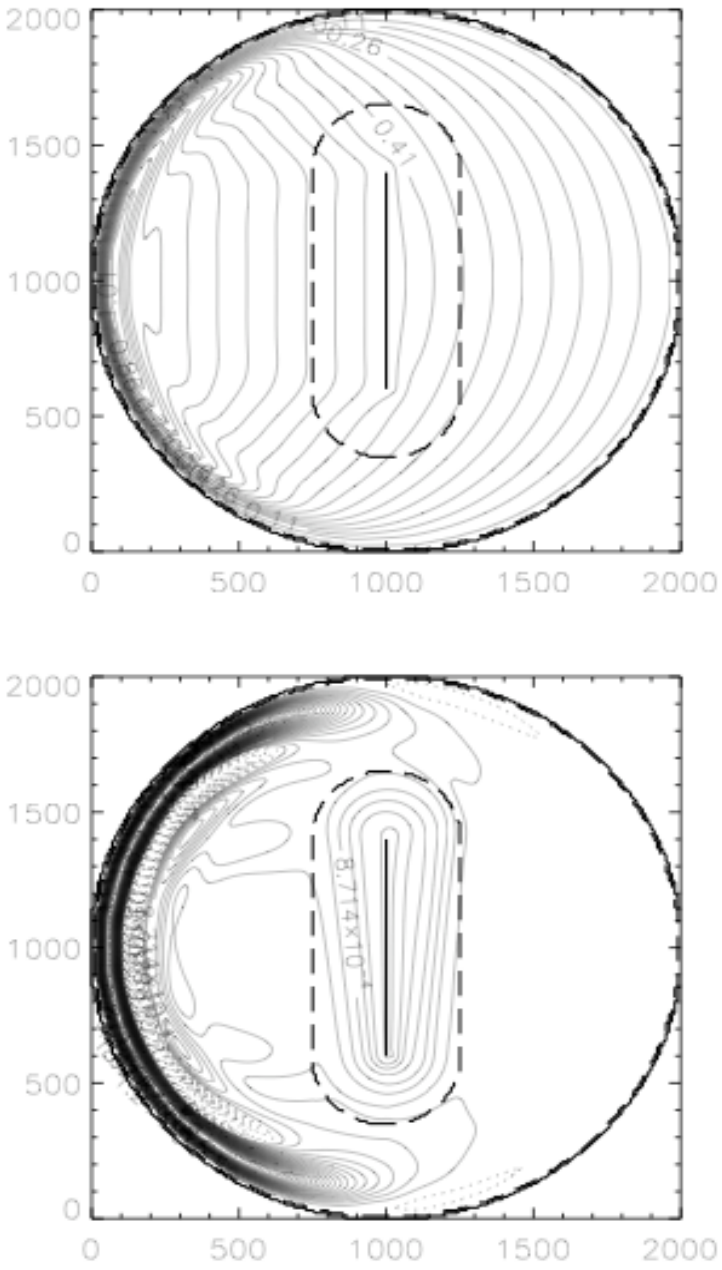

Figure 9 Steady state stream functions for the two layers (upper layer above), from a simulation with an island of 800 km, surrounded by a skirt of 250km , 600 m tall, whose boundary is indicated by the dashed contour. The contour intervals are 0.05 Sv and 2.5 x 10^{-4} Sv, respectively. The lower layer pattern displays a closed circulation around the island, over the skirt, with streamlines closely following the contours of constant potential vorticity.

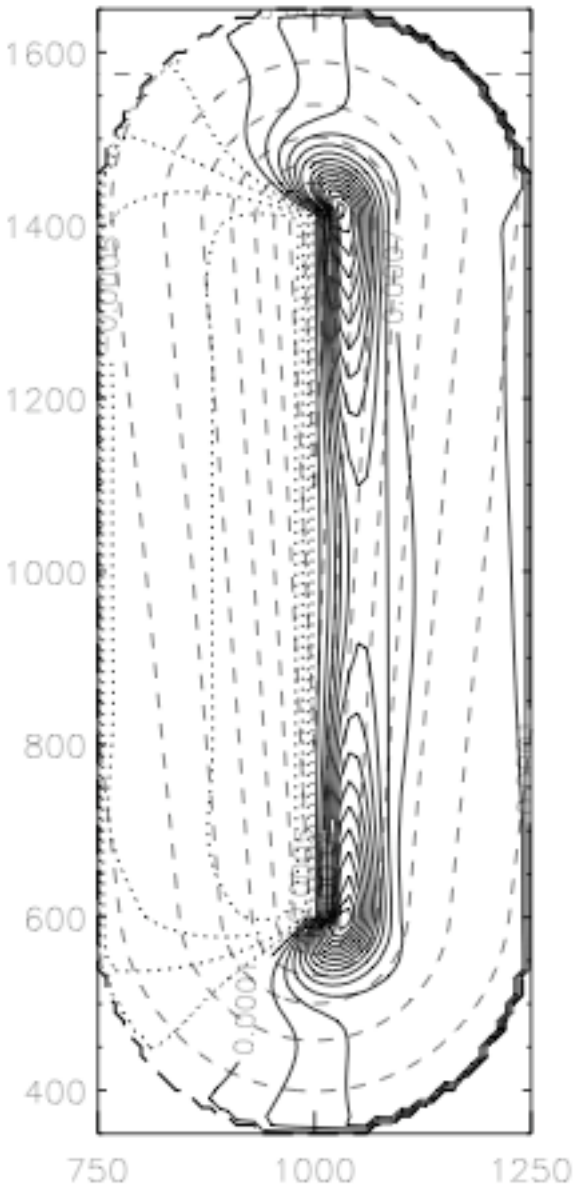

Figure 10 The integrand in the numerator of (3.7), measuring the strength of the forcing exerted by the upper layer, wind-driven dynamics, on the lower layer circulation. Equally spaced contours, with the solid (dotted) lines corresponding to anticyclonic (cyclonic) forcing, with the dashed lines indicating contours of constant potential vorticity.

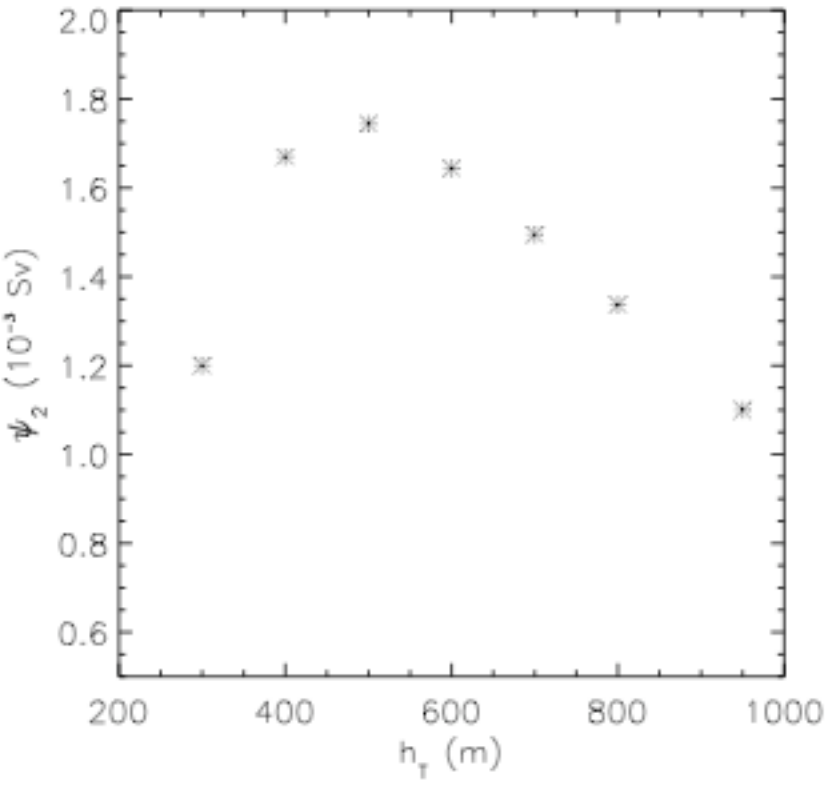

Figure 11 The dependence of the transport on the topographic height h_{T} for the meridional island.

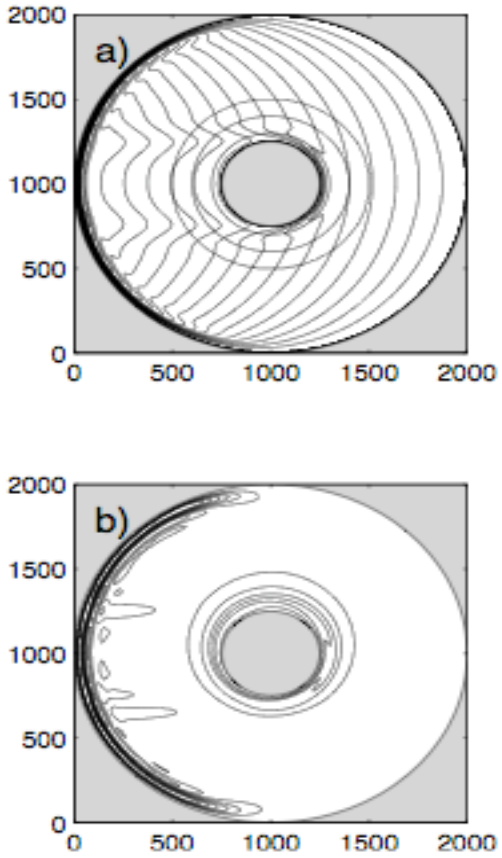

Figure 12 Mean streamfunction for a) upper layer and b) lower layer for δ_M = 10 km, δ_I = 2 km, λ_I = 10^{-5} m s^{-1}, r_I = 250 km, r_T = 500 km, and r_O = 1000 km. The streamfunction in both layers has been nondimensionalized by the upper layer island constant Ψ_I = .095 Sv, and the contour interval in a) is 0.1 and in b) is .004. The topography is indicated on a) by the gray circular contours, contour interval 200 m.

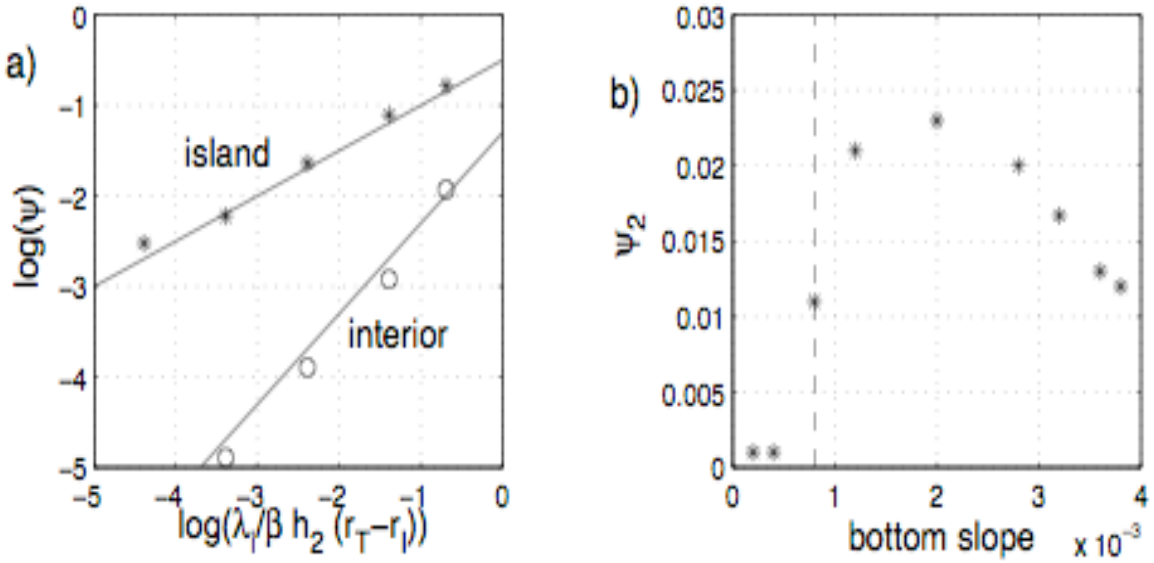

Figure 13 a) The total nondimensional transport over the topographic skirt (asterisks) and flat interior east of the topography (circles) as a function of the scaled coupling coefficient $\lambda_i / \beta h_2 (r_T - r_I)$. The straight lines have slopes proportional to $\lambda_i^{1/2}$ for the island result and λ_i for the interior result. b) The nondimensional transport over the skirt as a function of the bottom slope; the vertical dashed line is the approximate value for which the closed potential vorticity contours vanish.

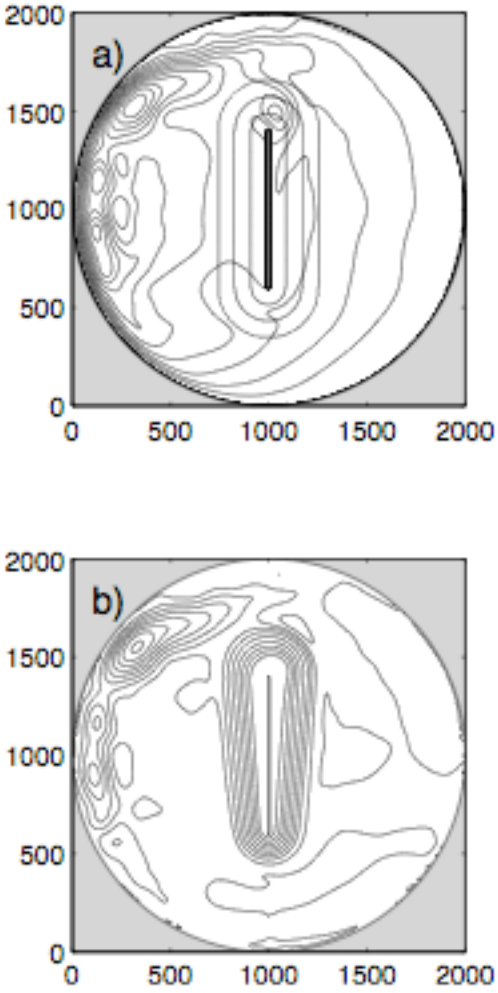

Figure 14 Mean a) upper and b) lower layer streamfunction from the final 5 years of a 20 year integration for the nonlinear numerical model. The streamfunction in both layers has been nondimensionalized by the upper layer island constant. The contour interval is 0.25. The bottom topography is indicated in a) by the gray contours, contour interval 200 m.